ABAI KAZAKH NATIONAL PEDAGOGICAL UNIVERSITY

ABAI CHEMICAL SCIENCES

Almaty, 2026

Kazakh National Pedagogical University named after Abai

«Abai Chemical Sciences»
№1 (1), 2026
Periodicity – 4 numbers in a year
Publishing from 2026.

050010, Almaty, Dostykave., 13
Abai KazNPU
Publishing house «Ulagat» Abai Kazakh National Pedagogical University

CONTENT

THERMAL AND CATALYTIC CRACKING OF NATURAL BITUMEN FROM THE MUNAILY-MOLA OIL SANDS

Khasanova A.[1], Tileuberdi Y.[2*]
[1]Individual Entrepreneur "Malina Agency", Astana, Kazakhstan
[2]Abai Kazakh National Pedagogical University, Almaty, Kazakhstan
[*]e-mail: er.tileuberdi@gmail.com

Abstract. In this study, the catalytic cracking of natural bitumen derived from the Munaily-Mola sands was investigated to enhance the production of light hydrocarbon fractions and synthetic liquid fuels. Catalytic cracking experiments were carried out in an autoclave reactor at 450 °C under steady-state conditions. Natural zeolite from the Taizhuzgen deposit was used as a catalyst due to its high adsorption capacity, ion-exchange properties, and catalytic activity. Prior to use, the zeolite catalyst was acid-treated and thermally activated to improve its surface acidity and catalytic performance. The material balance of the cracking process, as well as the group and fractional compositions of the obtained products, were analyzed. The results demonstrate that the use of natural zeolite significantly improves the efficiency of the cracking process by increasing the yield of liquid products while reducing coke formation. The yield of liquid hydrocarbons increased in the presence of the zeolite catalyst. Additionally, the catalytic process promoted the formation of lighter fractions and reduced the content of heavy residues. These findings confirm the potential of natural zeolite catalysts for upgrading heavy hydrocarbon resources and producing valuable liquid fuels from natural bitumen.

Keywords: catalytic cracking, oil sands, natural bitumen, beke deposits, natural zeolite.

Introduction

The basic trends in the development of current oil refining industry are caused by the need for increasing the depth of petroleum conversion and by more rigid ecological requirements imposed on oil refining processes and products [1]. The international oil refining industry is currently characterized by a decrease in light oil reserves and an increase in the fraction of the production and processing of heavy petroleum residues and oil bituminous rocks. Because of a decrease in production and an increase in the prime cost of light oils, the production of raw materials for the manufacture of petroleum products becomes a problem of increasing current interest [2].

The processing of oil bituminous rocks, which should be considered as a source of natural bitumens, promising hydrocarbon raw materials, is a developing branch of petroleum refining. One of the most important problems related to the processing of natural bitumens is a high concentration of high molecular weight compounds (tars and the asphaltenes, whose molecules concentrated a large part of heteroatoms present in the source material) in these bitumens. The amount of tars and asphaltenes is responsible for the properties of both a dispersion medium and a dispersed phase and the aggregative stability of natural bitumens under the conditions of thermolysis [3]. These compounds have high molecular weights; they are prone to condensation and coke formation upon processing, and they deactivate catalysts. The development of methods for the deep destruction of the tarasphaltene components of heavy oils and natural bitumens will make it possible to solve the main problem of the processing of heavy hydrocarbon raw materials and will reduce the scarcity of hydrocarbon fuel in the future.

The thermal destruction processes of heavy hydrocarbon raw materials make it possible to increase the yield of low boiling liquid products with the formation of coke and gas as by products. Cracking processes in the presence of different catalysts are of special interest. The thermocatalytic conversion of heavy hydrocarbon raw materials with iron oxide additives is a promising method for the production of synthetic oil. Microspheres, which can initiate the deep destruction of high molecular weight components, exhibited high efficiency in the processes of cracking [4, 5]. According to patent data, it is well known that the catalysts based on iron oxides, both synthetic and of technogenic or ore origin, exhibit activity in the processes of the steam cracking and hydrocracking of crude heavy oils [6].

The aim of this work was Processing of heavy oils of the Republic of Kazakhstan in the presence of zeolite catalyst by the thermocatalytic cracking method and obtaining its light oil products.

Materials and methods

The natural bitumen of oil sands from the deposits Munaily-Mola were used as heavy hydrocarbons.

As a catalyst we used zeolite (figure 1) from Taizhuzgen deposit. Zeolite is a unique natural mineral that has the property of absorbing and firmly retaining in its structure particles of various substances. Natural zeolite is an effective and cheaper substitute for artificial, as well as some natural mineral compounds. Therefore, in such technological processes, where the use of synthetic zeolites is unprofitable, the use of natural materials is of great importance. The industrial value of natural zeolite is determined by the presence of unique molecular and catalytic properties due to crystal-chemical characteristics, the ability to cation exchange, the loss and absorption of water and other molecules without destroying the structural framework. Zeolites are materials with an ever-expanding range of structures, compositions and uses. In Kazakhstan, several deposits of zeolites have been explored, the main indicators of which are identical to the known deposits of Ukraine (Sokirnitskoye), Georgia (Tedzamskoye) and Russia (Kholinskoye, Kulikovskoe, Vanginskoye). Map of the explored deposits of natural zeolites in the CIS countries Two large zeolite deposits are known in Kazakhstan: the Taizhuzgen.

Figure 1– Zeolite catalyst

Zeolite was prepared by preliminarily grinding and sifting the particles through molecular sieves with a size of until 0.25 mm. Ion exchange of the zeolite was carried out with 0.1 M HCl solution in a quartz column in a stirring mode in a boiling in-water bath for 6 hours. After acid treatment, the zeolite was filtered, washed with distilled water from chlorine ions by reaction with silver nitrate, dried successively in air at 100 °C until steady weight. Then they were subjected to thermal treatment in the air current in the temperature range 100-500°C for 3.5 hours. The catalyst was crushed to a particle size of 0.25 mm.

The acid properties of the catalysts were determined by the IRS method of adsorbed CO from the number of bands observed in the spectrum corresponding to the number of types of Lewis and Brunsted adsorption centers. The concentration of Lewis centers was measured from the integrated intensity of bands of adsorbed CO:

$$N\ [\mu mol / g] = A / A_0 \qquad (1)$$

where A is the integrated intensity of the band of adsorbed CO; A_0 is the coefficient of integral absorption.

Determination of the specific surface area of the catalyst samples was carried out on a ASAP 2400 Micrometrics (USA) specific surface area analyzer by low-temperature nitrogen adsorption using the BET method.

Thermocatalytic cracking of heavy under steady-state conditions was carried out in autoclave reactors with a volume of 12 ml. The mass of the bitumen loaded into the reactor was 7 g. The experiments were carried out in the air environment, which does not lead to significant changes in the composition of the resulting products due to its small volume, at a temperature of 450 °C and a duration of 60, 100 and 120 minutes. During the experiments, first was fixed the mass of the reactor without a sample and the second was fixed the mass of the reactor with the sample prepared for cracking. After thermal processing of natural bitumen, the yield of gaseous products was determined by the loss of mass of the reactor with the sample after removal of the gas products from the reactor. After separation products, the reactor was washed with

chloroform and weighed. The difference between the reactor mass before and after the experiment was determined as solid products (coke). Cracking initiated by ferrospheres was also carried out in autoclaves with a volume of 12 cm^3, where the admixture of bitumen charged to the reactor was 7 g, the addition of ferrospheres was 10% by weight. The experiments proceeded as described above with the only difference - the cracking products were filtered to separate the liquid part from the ferrosphere. After the cracking, the filtered ferrospheres were weighed. The sum of the differences obtained between the weight of the reactor and the ferrospheres before and after the experiment was determined as solid products.

Experiments with the HY zeolite were carried out in autoclaves. Pre-bitumen with catalyst was homogenized and placed in an autoclave, the bitumen charge was 7 g, and the amount of catalyst was 0.5, 1 and 1.5% by weight. Figure 2 shows the installation.

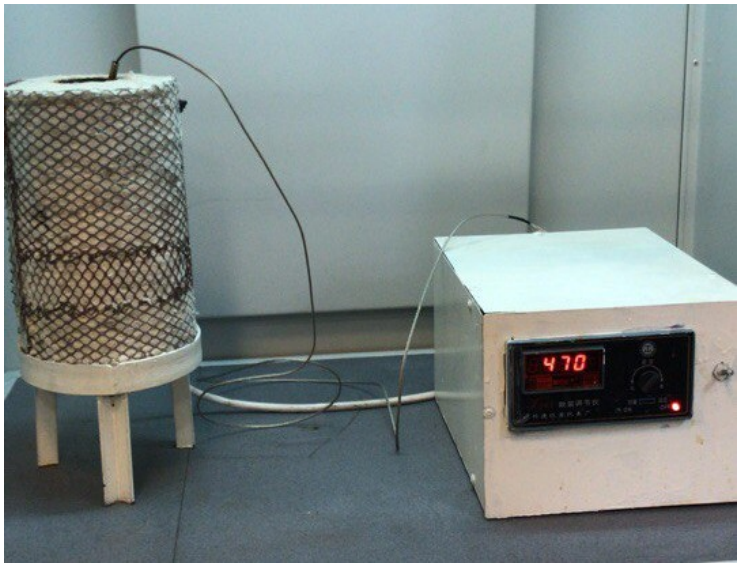

Figure 2 – Picture installation made in laboratory

Results and discussion

The table chart gives information of number of content, as gas, coke and liquid products after different processes and compares the percentage of products without catalyst and with catalyst.

Table 1 - Material balance of the process of thermal catalytic cracking of Natural bitumen of the Munaily-Mola deposit in steady state

Process	Content, wt. %		
	Gas	Coke	Liquid products
Initial bitumen	0	0	100,0
Cracking	0,2	26,2	73,6
Cracking with natural zeolite	1,2	13,4	85,4

Overall, it is clear from the table that amount of gas and liquid products have an upward trend in cracking process, however, the number of cokes decreased gently from 26.2 to 13.4 per cent. To sum up, using a catalyst is great opportunity to improve liquid products and reduce solid parts of heavy oil.

The bar chart (figure 3) below compares the number of the products between initial bitumen, cracking and cracking with catalyst of natural bitumen of the Munaily-Mola deposit (Figure 4).

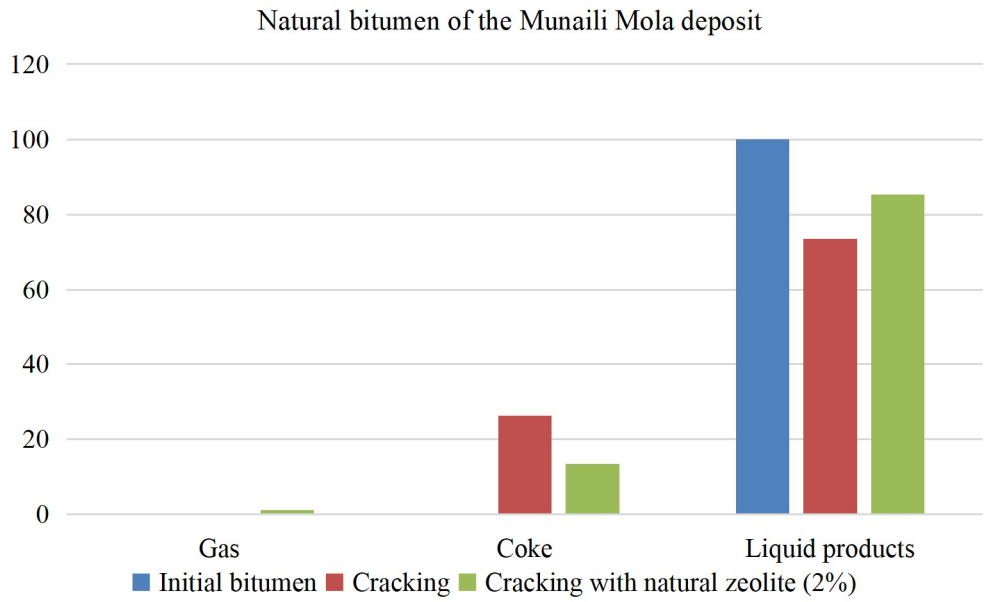

Figure 3 – Bar chart of Material balance of the process of thermal catalytic cracking of Natural bitumen of the Munaily-Mola deposit

As can be seen from the given bar chart our zeolite catalyst improved the goal product (liquid) and gas, while at the same time scaled down the amount of cake in around two times.

Figure 4 – Picture sample after cracking

The table 2 gives information about component composition of products of thermocatalytic cracking of Natural bitumens of the Munaily-Mola deposit. Overall, it is clear from the chart that the percentage of oils and asphaltenes showed an upward trend and the percentage of tars dipped down. However, natural bitumens from Munaily-Mola deposits illustrated better characteristics after thermocatalytic cracking in the amount of asphaltenes, which increased nearly in three times.

Table 2 - Component composition of products of thermocatalytic cracking of Munaily-Mola natural bitumen

Process	Content, wt. %		
	Oils	Tars	Asphaltenes
Initial bitumen	47,6	46,4	6,0
Cracking	83,6	13,4	3,0
Cracking with natural zeolite	61,5	27,3	11,2

Table 3 shows fractional composition of products of thermocatalytic cracking of natural bitumen of the Munaily-Mola deposit in steady state. As can be seen from the chart cracking with natural zeolite improved light fraction and middle fraction and decreased heavy fraction of given natural bitumen oil sand. However, this sample of natural bitumen from Munaily-Mola deposit illustrates better percentage of fractional composition.

Table 3 - Fractional composition of products of thermocatalytic cracking of bitumens

Process	Content, wt. %		
	<-200°C	200-360 °C	>360 °C
Initial bitumen	2,2	15,6	82,2
Cracking	9,3	34,2	56,5
Cracking with natural zeolite	15,5	38,2	46,3

Conclusion

The present study investigated the thermocatalytic cracking of natural bitumen obtained from the Munaily-Mola oil sands using natural zeolite as a catalyst. The increasing demand for light petroleum products and the gradual depletion of conventional crude oil resources make the processing of heavy hydrocarbon feedstocks an important technological and economic challenge. Natural bitumen, which contains a significant amount of high-molecular-weight components such as resins and asphaltenes, requires effective upgrading methods to convert it into lighter and more valuable hydrocarbon fractions.

The experimental results demonstrated that the application of natural zeolite significantly enhances the efficiency of the cracking process. Compared with thermal cracking without catalyst, catalytic cracking in the presence of zeolite resulted in a higher yield of liquid products and a considerable reduction in coke formation.

The analysis of group composition revealed that the catalytic process promotes the transformation of heavy resin-asphaltene components into lighter oil fractions. The proportion of oils in the products increased significantly, while the content of tars decreased. Furthermore, the fractional composition analysis showed a notable increase in light and middle distillate fractions, accompanied by a reduction in heavy fractions. These changes indicate the effective breakdown of high-molecular-weight hydrocarbons during catalytic cracking. The findings of this study provide a scientific basis for the further development of catalytic technologies for processing oil sands and other unconventional hydrocarbon feedstocks in Kazakhstan.

References

1. Joshi, J. B., Pandit, A. B., Kataria, K. L., et al. (2008). Industrial & Engineering Chemistry Research, 47(23), 8960.

2. Ongarbayev, Y. K., Tileuberdi, E., Tuleutaev, B. K., & Mansurov, Z. A. (2013). Neftepererabotka i Neftekhimiya, (3), 12.

3. Kopytov, M. A., & Golovko, A. K. (2009). Izvestiya Tomskogo Politekhnicheskogo Universiteta, 315(3), 83.

4. Kizil'shtein, L. Ya., Dubov, I. V., Shpitsgluz, A. L., & Parada, S. G. (1995). Komponenty zolishlakov TES (Thermal Power Plant Ash and Slag Components). Moscow, Russia: Energoatomizdat.

5. Kopytov, M. A., Golovko, A. K., Kirik, N. P., & Anshits, A. G. (2013). Neftekhimiya, 53(1).

6. Murakami, T., Suzuka, T., Inoue, Y., & Aizawa, S. (1983). U.S. Patent No. 4,421,635.

FACILE FABRICATION OF MAXENE/SIC-BASED ELECTROCHEMICAL INK ELECTRODES

Mukataeva Zh.S.[1], Bakytkarim Y.[1], Konarbay D.B.[1], Shadin N.A.[1], Akylbekova T.N.[1]
[1]Abai Kazakh National Pedagogical University, Almaty, Kazakhstan
*e-mail: zh.mukatayeva@abaiuniversity.edu.kz

Abstract. In this work, MAXene/SiC-based conductive ink electrodes were successfully fabricated using a simple and low-cost direct writing method. MAXene nanomaterials were synthesized and combined with silicon carbide (SiC) nanoparticles to prepare conductive electrochemical ink. Chitosan solution was used as a binder to improve the adhesion stability of the electrode materials on the substrate surface. The obtained ink was manually written onto a PVC substrate to form electrochemical electrodes and dried at room temperature. The fabricated electrodes demonstrated good film formation and conductive properties, indicating the potential of MAXene/SiC composite materials for electrochemical applications. The proposed approach provides a facile strategy for the development of flexible and low-cost electrochemical platforms.

Keywords: MAXene, silicon carbide, conductive ink, electrochemical electrode, direct writing, nanocomposite, flexible electrode, chitosan.

Introduction

Recently, electrochemical electrodes based on nanomaterials have attracted significant attention due to their excellent electrical conductivity, large surface area, and promising electrochemical performance. Among various nanomaterials, MAXene has emerged as a highly attractive two-dimensional material because of its unique layered structure, hydrophilicity, and superior electrical properties. In addition, silicon carbide (SiC) nanoparticles possess high chemical stability, mechanical strength, and thermal resistance, making them suitable for electrode fabrication. Conductive ink technology has become an important approach for the fabrication of flexible and portable electrochemical devices. Compared with conventional electrode preparation methods, direct writing techniques offer several advantages, including simplicity, low cost, and easy processing. Therefore, the development of MAXene-based conductive ink electrodes is of considerable interest for future electrochemical applications.

In this study, MAXene and SiC nanoparticles were used to prepare conductive electrochemical ink. The electrodes were fabricated on PVC substrates using a simple brush-writing method with chitosan as a binder. The morphology and electrochemical properties of the fabricated electrodes were investigated to evaluate their potential application in electrochemical systems.

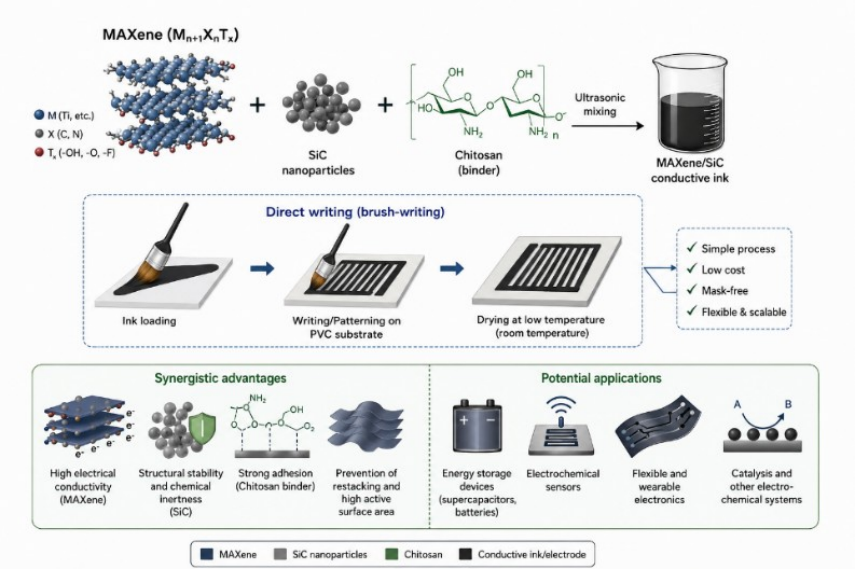

Figure 1 - Schematic illustration of MAXene/SiC conductive ink preparation and brush-written electrode fabrication process

MAXene is one of the new-generation nanomaterials with a two-dimensional structure. It belongs to the family of transition metal carbides, nitrides, and carbonitrides. Since its first discovery in 2011, MAXene has attracted significant attention from researchers. The general formula of MXene is expressed as $M_{n+1}X_nT_x$, where M represents a transition metal, X refers to carbon and/or nitrogen, and Tx denotes surface functional groups such as -OH, -O, and –F [1]. The presence of these functional groups improves the hydrophilicity of MAXene and allows it to disperse well in various solutions. In addition, the metallic layers provide excellent electrical conductivity. Due to its outstanding electrochemical, mechanical, electronic, and optical properties, MAXene has been widely used in energy storage devices, sensors, electronics, biomedicine, and catalysis [2].

After the exfoliated layers are uniformly dispersed in solvents and mixed with additional components, functional inks suitable for printing can be obtained. Such inks make it possible to fabricate electrochemical devices using simple and efficient methods. In recent years, printing technologies have been widely applied in the development of energy storage systems due to their advantages, including simple fabrication process, low cost, and suitability for large-scale production [3]. Selecting an appropriate printing method is an important step in the fabrication of electrochemical devices. Different printing technologies vary in printing resolution, film thickness, and processing speed. Therefore, the properties of the prepared ink should be compatible with the selected printing technique. To improve the stability of the ink and ensure uniform deposition on the substrate surface, various binders and additives are commonly introduced into the ink composition [4].

In addition, thermal treatment is often used to remove excess additives from the material. However, high-temperature processing may affect the material properties and complicate the fabrication procedure. For this reason, increasing attention has been focused on conductive inks that can be processed at low temperatures and easily deposited onto flexible substrates. Previous studies have reported that inks based on graphene, black phosphorus, molybdenum disulfide, and MXene exhibit promising performance on various substrates [5].

Silicon carbide (SiC) is another promising material that has attracted increasing attention in electrochemical and electronic applications due to its excellent thermal stability, high mechanical strength, chemical inertness, and semiconductor properties [6]. Compared with conventional carbon-based nanomaterials, SiC nanoparticles exhibit superior resistance to corrosion and oxidation, making them suitable for harsh operating environments. In addition, the incorporation of SiC nanoparticles into conductive composites can improve structural stability and increase the active surface area of electrode materials. Owing to these advantages, SiC-based materials have been widely investigated in sensors, energy storage devices, catalytic systems, and electronic applications [7].

Recently, the combination of MAXene with other nanomaterials has become an effective strategy to enhance the functional properties of conductive composites. In particular, hybrid materials based on MAXene and ceramic nanoparticles demonstrate improved electrochemical stability and mechanical durability [8]. The layered structure of MAXene provides efficient pathways for electron transport, while SiC nanoparticles can prevent the restacking of MAXene sheets and maintain the accessibility of active sites. Therefore, the development of MAXene/SiC composites is considered a promising approach for fabricating conductive inks and electrochemical electrodes.

Another important aspect in the fabrication of conductive inks is the selection of suitable binders and substrates. Chitosan has attracted attention as a biodegradable and environmentally friendly polymer due to its excellent film-forming ability and adhesive properties [9]. The presence of amino and hydroxyl functional groups in chitosan promotes strong interaction between the conductive material and the substrate surface. As a result, chitosan is widely used as a binder in electrochemical and printed electronic applications. Furthermore, flexible substrates such as polyethylene terephthalate (PET), paper, textiles, and polyvinyl chloride (PVC) are commonly employed for printed electrodes because of their low cost, lightweight nature, and mechanical flexibility [10].

Among various fabrication techniques, direct writing methods have emerged as simple and efficient approaches for producing flexible electrochemical devices. Unlike conventional lithographic and vacuum-based methods, brush writing does not require expensive equipment or complicated processing steps. This method enables rapid deposition of conductive materials onto different substrates and allows the fabrication of customizable electrode patterns. In addition, direct writing techniques are compatible with large-area and low-temperature processing, which is important for flexible and wearable electronic systems [11].

Previous studies mainly focused on MAXene-based inks for supercapacitors, microsupercapacitors, and printed electronics applications [12]. However, studies related to MAXene/SiC-based conductive ink electrodes prepared by simple brush-writing methods are still limited. Therefore, developing low-cost conductive electrodes based on MAXene and SiC nanoparticles remains an important research direction in the field of electrochemical materials.

In this work, MAXene/SiC conductive ink was successfully prepared and applied for the fabrication of electrochemical electrodes on PVC substrates. The prepared materials were characterized using morphological analysis, and the feasibility of the fabricated conductive electrodes for electrochemical applications was evaluated. The proposed fabrication approach provides a simple and cost-effective strategy for the development of conductive materials for future printed and flexible electrochemical devices [13].

Materials and methods

Synthesis methods of MAXene and ink formulation

To develop MXene-based electrochemical materials, comprehensive studies are carried out involving the synthesis of nanomaterials, investigation of their structural and morphological properties, fabrication of modified electrodes, and evaluation of their electrochemical characteristics. The research includes several interconnected directions.

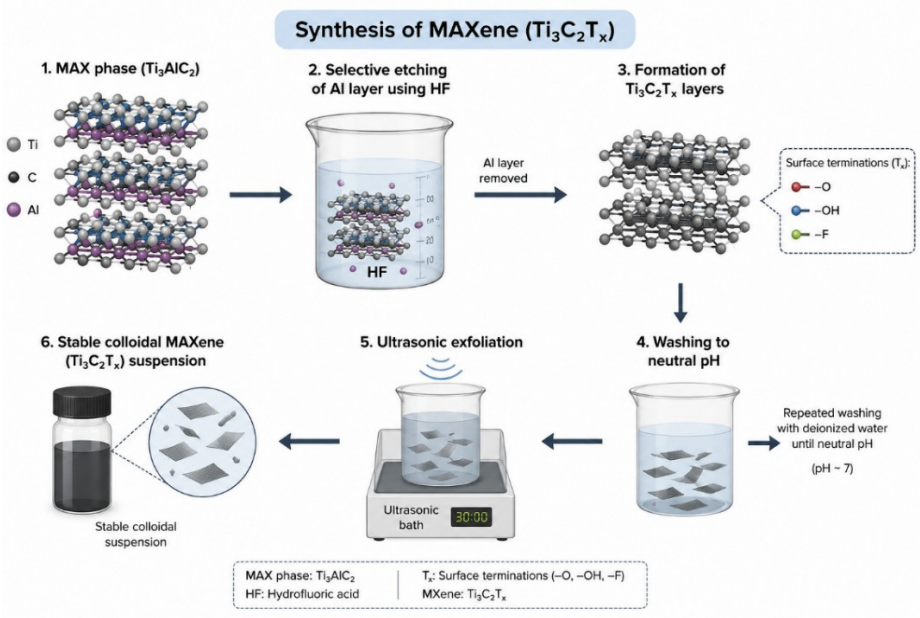

Figure 2 - Synthesis of MAXene

The synthesis process of the MAXene nanomaterial is illustrated in Figure 2. MAXene is obtained by selectively removing the aluminum layer from the layered MAX phase (Ti_3AlC_2). For this purpose, hydrofluoric acid (HF) is used. During the etching process, the aluminum atomic layers in the Ti_3AlC_2 structure are dissolved, resulting in the formation of a two-dimensional $Ti_3C_2T_x$ material. Here, T_x represents the surface functional groups such as –O, –OH, and –F. After synthesis, the obtained product is repeatedly washed and purified until a neutral medium is reached. Subsequently, ultrasonic treatment is applied to promote the delamination of the layers. As a result, a stable colloidal MAXene suspension is obtained.

Preparation of electrode ink

100 mg of SiC nanoparticles and 100 mg of MXene were dispersed in 10 mL of ultrapure water and ultrasonicated for 30 min to obtain the working electrode ink. Meanwhile, silver nanowires with a concentration of 20 mg/mL were dispersed in 10 mL of ultrapure water to prepare the reference/counter electrode ink. To ensure strong adhesion of the electrode materials onto the substrate surface, chitosan solution was used as a binder. For this purpose, 50 mg of chitosan was dissolved in 10 mL of 0.1 M acetic acid solution.

Preparation of electrochemical sensor

As shown in Figure 3, the working and reference/counter electrode inks, together with the chitosan solution, were sequentially written onto a solid substrate (such as PVC) using a brush. The prepared electrodes were then dried at room temperature for 20 min. Finally, the electrodes were cut into small pieces with dimensions of 3 mm × 3 mm for further use. The electrochemical system was based on a two-electrode configuration.

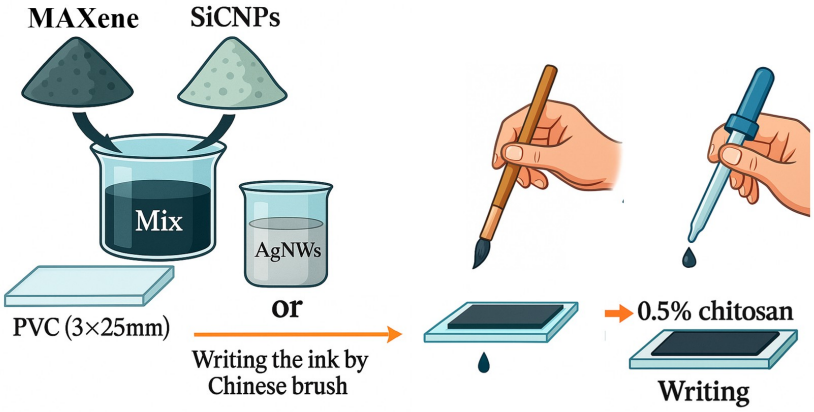

Figure 3 - Fabrication process of MAXene/SiC NPs-CS and reference/counter electrode

The MXene/SiC-based conductive ink electrodes were successfully fabricated using the brush-writing method (Figure 4). The prepared electrodes formed a uniform coating layer on the PVC substrate and exhibited good mechanical stability. No visible cracks or delamination were observed on the electrode surface, indicating that the chitosan binder effectively improved the adhesion of the material onto the substrate surface. In addition, the compact size and simple fabrication process of the obtained electrodes demonstrate their potential applicability in electrochemical devices.

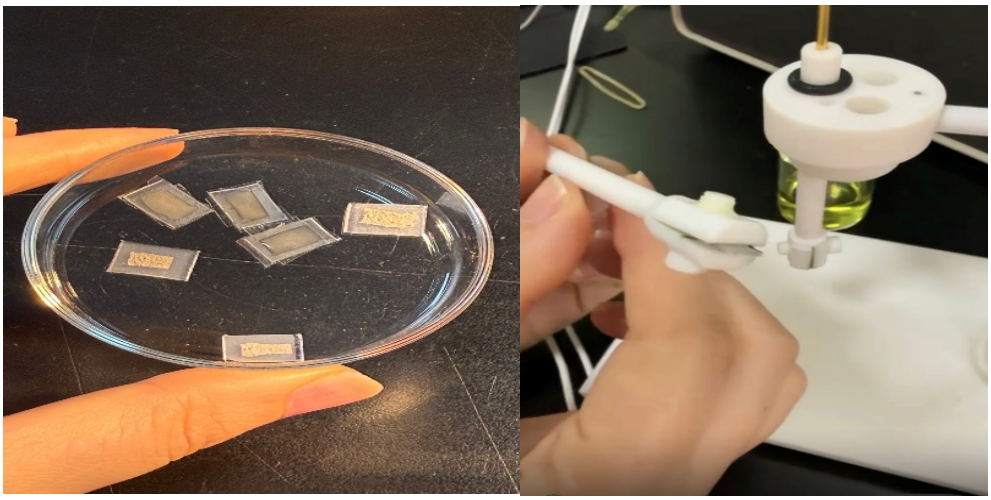

Figure 4 - Fabricated MAXene/SiC-based conductive ink electrodes

Results and discussion

The SEM images show the morphology of the synthesized MAXene/SiC composite material. The obtained images reveal the structural features and surface morphology of the composite. A layered and sheet-like structure characteristic of MAXene can be clearly observed. The interconnected layered morphology confirms the two-dimensional nature of the MAXene material. In addition, granular particles with different sizes are distributed on the surface, indicating the successful incorporation of SiC nanoparticles onto the MAXene sheets.

According to the SEM results, the surface of the composite exhibits a rough and relatively developed morphology (Figure 5). Such a structure can contribute to an increased specific surface area of the material. Furthermore, the SiC nanoparticles located between the MAXene layers may reduce the restacking of the sheets, which can positively influence the stability and conductivity of the composite. The higher magnification SEM image demonstrates that the SiC nanoparticles are distributed on the surface and between the layers of the MAXene sheets. The relatively uniform distribution of the particles confirms the successful synthesis of the MXene/SiC composite. The absence of large agglomerates suggests that the synthesis process was carried out effectively.

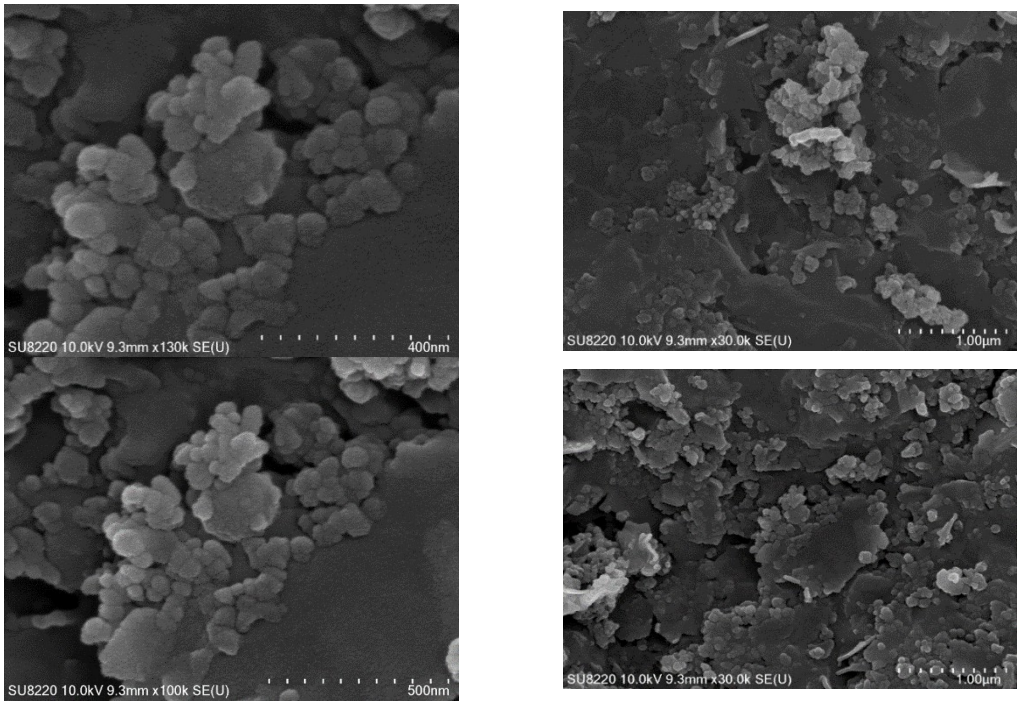

Figure 5 - SEM characterization of the synthesized MAXene/SiC nanocomposite structure

Overall, the SEM analysis indicates that the MAXene/SiC composite possesses a layered structure with well-dispersed SiC nanoparticles interacting with the MXene surface. Such structural characteristics make the material promising for electrochemical applications.

The synthesized MAXene material was successfully obtained by selective etching of the Al layer from the Ti_3AlC_2 MAX phase using HF solution. After the etching process and ultrasonic treatment, a stable MXene suspension was formed, indicating the successful delamination of the layered structure. The obtained MAXene exhibited good dispersibility in aqueous solution due to the presence of surface functional groups. The morphology and surface structure of the synthesized MAXene/SiC composite were investigated using SEM analysis. As shown in Figure 4, the material exhibited a typical layered and sheet-like structure characteristic of MAXene. The SEM images also revealed that the SiC nanoparticles were distributed on the surface and between the MAXene layers. The incorporation of SiC nanoparticles contributed to the formation of a rough and developed surface morphology, which may enhance the active surface area of the material.

In addition, the layered MAXene structure provided conductive pathways for electron transfer, while the SiC nanoparticles could improve the structural stability of the composite. The relatively uniform distribution of SiC particles on the MAXene sheets indicates the successful formation of the MAXene/SiC nanocomposite. No significant agglomeration was observed in the SEM images, suggesting that the synthesis and dispersion processes were effective. The prepared MAXene/SiC conductive ink showed good adhesion to the PVC substrate with the assistance of chitosan binder. The brush-writing method allowed the facile fabrication of electrochemical electrodes with a relatively uniform coating layer. After drying at room temperature, the fabricated electrodes maintained good structural integrity without visible cracks on the surface. Overall, the obtained results demonstrate that the MAXene/SiC composite is a promising material for conductive ink and electrochemical electrode fabrication. The simple preparation procedure and

favorable structural properties indicate its potential application in future electrochemical devices and flexible electronic systems.

Conclusion

In this work, a MAXene/SiC-based conductive composite was successfully prepared, and its potential application as an electrochemical ink was investigated. The layered structure of MAXene together with the stability of SiC nanoparticles contributed to the improvement of the functional properties of the composite. In addition, the use of chitosan as a binder provided good adhesion of the material onto the substrate surface.

The proposed brush-writing method demonstrated a simple and accessible approach that does not require complex equipment. Using this method, electrochemical electrodes can be fabricated in a short period of time. The structural characteristics of the prepared materials indicate their suitability for electrochemical applications.

Overall, MAXene/SiC-based conductive inks represent a promising direction for the fabrication of electrochemical materials. In the future, such materials may find potential applications in sensor platforms, flexible electronics, and printed technologies.

References

1. Lin, Z.; Li, X.; Zhang, H.; et al. Research progress of MXenes and layered double hydroxides for supercapacitors. Inorg. Chem. Front. 2023, 10, 4358-92. https://doi.org/10.1039/D3QI00819C

2. Lamiel, C.; Hussain, I.; Warner, J. H.; Zhang, K. Beyond Ti-based MXenes: a review of emerging non-Ti based metal-MXene structure, properties, and applications. Mater. Today. 2023, 63, 313-38. https://doi.org/10.1016/j.mattod.2023.01.020

3. Jun, H. Y.; Ryu, S. O.; Kim, S. H.; et al. Inkjet printing of few-layer enriched black phosphorus nanosheets for electronic devices. Adv. Elect. Mater. 2021, 7, 2100577. https://doi.org/10.1002/aelm.202100577

4. Li, L.; Meng, J.; Bao, X.; et al. Direct-ink-write 3D printing of programmable micro-supercapacitors from MXene-regulating conducting polymer inks. Adv. Energy. Mater. 2023, 13, 2203683. https://doi.org/10.1002/aenm.202203683

5. Shao, Y.; Wei, L.; Wu, X.; et al. Room-temperature high-precision printing of flexible wireless electronics based on MXene inks. Nat. Commun. 2022, 13, 3223. https://doi.org/10.1038/s41467-022-30648-2

6. Li Z., Wang X., Zhang Y. Multifunctional MXene inks for printed electrochemical energy storage devices // Energy Materials. – 2025. – Vol. 5. 10.20517/energymater.2024.31.

7. Ko T.Y., Kim Y., Lee J. Functionalized MXene ink enables environmentally stable printed electronics // Nature Communications. – 2024. – Vol. 15. – P. 3459. 10.1038/s41467-024-47700-y.

8. Htwe Y.Z.N., Kim S., Lee H. Progress in etching-driven MXene synthesis and utilization in conductive inks for printed electronics applications: A comprehensive review // Synthetic Metals. – 2024. – Vol. 306. – P. 117631. 10.1016/j.synthmet.2024.117631.

9. Aghayar Z., Hassanpour A., Faghihi S. MXene-Based Ink Design for Printed Applications // Nanomaterials. – 2022. – Vol. 12, № 21. – P. 3859. 10.3390/nano12213859.

10. Cao W., Wang Y., He P. A Highly Stable MXene Aqueous Conductive Ink for Inkjet Printing Flexible Microsupercapacitors // ACS Applied Materials & Interfaces. – 2021. – Vol. 13. – P. 10754–10762. 10.1021/acsami.1c00724.

11. Thirumal V., Arunachalam P., Raja A. Binder-Free Two-Dimensional Few-Layer Titanium Carbide MXene Conductive Inks // Crystals. – 2024. – Vol. 14. – P. 261. 10.3390/cryst14030261.

12. Wu Z., Li M., Chen J. MXene Contact Engineering for Printed Electronics // Advanced Functional Materials. – 2023. – Vol. 33. 10.1002/adfm.202301245.

13. Redondo E., Chao M., Bahamonde A. MXene-functionalised 3D-printed electrodes for electrochemical capacitors // Journal of Electroanalytical Chemistry. – 2021. – Vol. 896. – P. 115178.10.1016/j.jelechem.2021.115178.

CATALYSIS ON IMMOBILIZED COMPLEXES FOR HYDROGENATION

Kurmanbayeva I.[1*], Selenova B.[2], Mukhamedzhanova S.[3], Zharmagambetova A.[3]
[1]Abai Kazakh National Pedagogical University, Almaty, Kazakhstan
[2]Satbayev University, Almaty, Kazakhstan
[3]D.V. Sokolsky Instytut of Fuel, Catalysis and Electrochemistry, Almaty, Kazakhstan
[*]e-mail: i.kurmanbayeva@abaiuniversity.edu.kz

Abstract. This review is dedicated to the memory of scientists Alima Kainekeevna Zharmagambetova and Sabira Gafurovna Mukhamedzhanova. It summarizes the fundamental principles for designing supported palladium–polymer complexes for hydrogenation reactions. Although the studies were conducted between 1975 and 2000, before the emergence of concepts such as enzymatic catalysis and green chemistry, the established approaches to selecting supports, polymer ligands, and synthesis conditions remain relevant. These principles enable the development of selective and stable catalysts that operate under mild conditions and exhibit prolonged catalytic lifetimes.

Keywords: hydrogenation, palladium-polymer complex, nanoparticle, catalyst, polyvinylpyridine

Introduction

The fundamental principle of immobilized complex catalysis is to develop catalysts that combine the advantages of homogeneous catalysts - such as high activity, selectivity, and efficient utilization of active sites - with those of heterogeneous catalysts, including high stability, convenient processability, and easy separation from reaction products. Table 1 summarizes the main characteristics of homogeneous and heterogeneous catalysts, highlights the differences between these catalytic systems, and presents the expected advantages of immobilized catalysts.

Table 1 - Comparison of various catalytic systems

Properties of catalysts	Homogeneous catalyst	Heterogeneous catalyst	Immobilized complexes
Activity	-	+	+
Typical operating range of catalytic systems	-	+	+, -
The possibility of multiple ions participating in the catalytic process	-	+	+, -
Stability	-	+	+
Ease of separation from the reaction products	-	+	+
Variation of ligands coordinated to the transition metal ion at the catalytic active site	+, -	-	+
Identification of active sites	+	-	+
Selectivity	+	-	+

There are two main types of supports used for complex immobilization: organic polymers and inorganic oxides. Polymer supports offer several advantages in catalysis due to their ability to readily form chemical bonds with metal ions. When the active phase of a catalyst is immobilized on the surface of a polymer support, a polymer–metal complex (PMC) is formed, in which the polymer acts as a macroligand.

The interest in PMCs is largely associated with their similarity to natural catalytic systems, particularly enzymes [1-3]. Many enzymes contain strongly bound metal ions, typically transition metals, and function in combination with coenzymes. The polymeric nature of enzyme molecules is essential for maintaining their three-dimensional structure and catalytic activity.

Polyvinylpyridine palladium complexes

Polymers containing functional groups are widely used for the immobilization of metal ions [4-7]. In many cases, even minor variations in the preparation method lead to significant differences in the catalytic activity of the resulting polymer–metal complexes (PMCs). Polyvinylpyridines are promising polymeric materials that can serve as catalytic supports. The polymer complexes P2VP–Pd(II) and P4VP–Pd(II) were synthesized by mixing ethanol solutions of $PdCl_2$ and the corresponding polymer at a 1:1 molar ratio, resulting in catalysts containing 1.2 wt.% Pd. The obtained precipitates were washed with ethanol and air-dried at room temperature. The polymer complexes were subsequently reduced with $NaBH_4$ in aqueous solution, washed with water, and evaluated in the hydrogenation of allyl alcohol. Palladium black was prepared by reducing $PdCl_2$ in aqueous solution using a twofold excess of $NaBH_4$.

Poly(2-vinylpyridine) (P2VP) and poly(4-vinylpyridine) (P4VP) contain nitrogen atoms in different positions within their pendant pyridine groups relative to the polymer backbone. The position of these functional groups influences the complexation ability of the polymers and, consequently, may affect their catalytic activity. P2VP is capable of forming coordination bonds between neighboring 2-vinylpyridine units, whereas P4VP predominantly forms intermolecular crosslinked structures. Based on the ability of $PdCl_2$ to form binuclear bridged complexes, the following structural models can be proposed for P4VP–Pd(II) (a) and P2VP–Pd(II) (b).

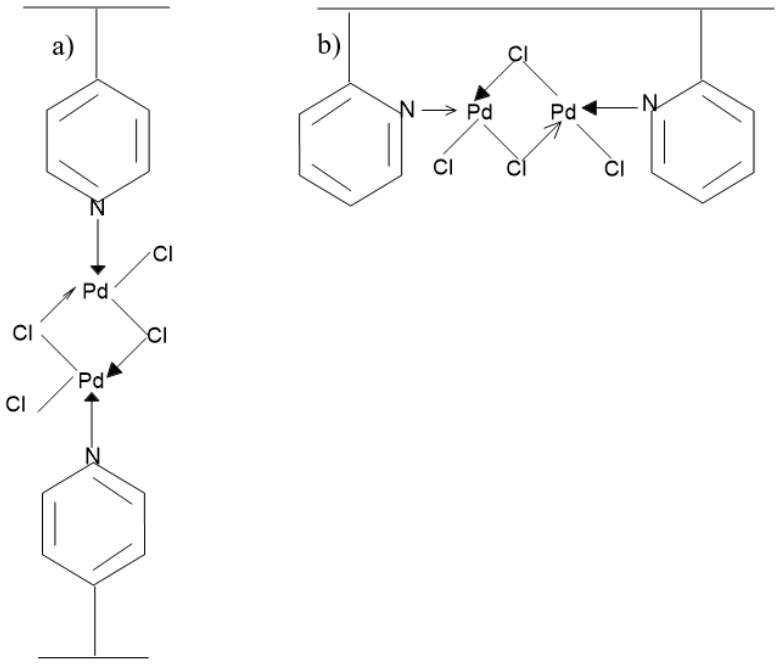

Figure 1 – Pd complexes with: a) P4VP, b) P2VP [adapted from 5]

Polyvinylpyridine (PVP) is readily soluble in ethanol. Mixing ethanol solutions of PVP and $PdCl_2$ forms yellow precipitates that gradually transform into swollen flakes upon prolonged stirring. The persistent yellow color of the mother liquor indicates incomplete palladium binding. Spectrophotometric analysis confirmed this observation. The N:Pd atomic ratios for P2VP–$PdCl_2$ and P4VP–$PdCl_2$ were 1.6 and 1.8,

indicating mixed-composition complexes in which palladium coordinates with one or two pyridine nitrogen atoms. Coordination with more than two polymer chains is sterically hindered. Reduction with $NaBH_4$ changes the complex color from yellow to gray, yielding complexes of the formula L_2PdCl_2. IR spectroscopy confirmed complex formation. Compared with the free ligands, the complexes showed deformation of the C=C and C=N bonds in the pyridine ring. Absorption bands at 1620 cm^{-1} for P2VP–$PdCl_2$ and 1612 cm^{-1} for P4VP–$PdCl_2$ indicate coordination between pyridyl nitrogen atoms and palladium.

Table 2 - Analytical and IR spectroscopic data for PVP–$PdCl_2$ complexes [4]

Catalyst	Contents (%)			Empirical atomic ratios		ν(C=C), ν(C=N) (cm^{-1})
	N	Pd	Cl	N/Pd	Cl/Pd	
Calculated values						
PVP	15.2	—	—	—	—	
PVP–$PdCl_2$	5.2	39.5	19.6	1	2	
$(PVP)_2$–$PdCl_2$	7.8	29.4	26.4	2	2	
Experimental values						
P2VP	14.0	—	—	—	—	1590
P2VP–$PdCl_2$	5.2	24.6	25.0	1.6	3.0	1620
P2VP–$PdCl_2$ ($NaBH_4$)	6.4	25.9	17.4	1.9	2.0	1600, 1590
P4VP	14.3	—	—	—	—	1596
P4VP–$PdCl_2$	6.5	27.0	24.0	1.8	2.7	1612
P4VP–$PdCl_2$ ($NaBH_4$)	6.6	28.5	18.3	1.9	1.9	1597, 1614

The vibrational bands shifted to higher frequencies, while $NaBH_4$-treated samples showed bands of both free and coordinated pyridine groups. This indicates partial cleavage of N–Pd bonds and partial reduction of Pd(II) under H_2 or $NaBH_4$ treatment. Treatment with H_2 or $NaBH_4$ reduced Pd(II) to Pd(0), with binding energies of 335.3 and 335.6 eV, respectively. H_2-reduced samples also showed a Pd $3d_{5/2}$ peak at 336.5 eV, attributed to Pd(I). Pd(II) species remained in both samples. After hydrogenation, the catalyst contained Pd(II) and Pd(0), whereas Pd(I) disappeared. Hydrogen treatment reduced 17% of palladium to Pd(0), while $NaBH_4$ produced only 4% Pd(0). After hydrogenation of 2-propen-1-ol, the Pd(0) content increased to 30–33%. These values may be uncertain because nanosized palladium particles (10–100 Å) can exhibit binding energies that differ from those of bulk metal.

Thus, studies of PVP–$PdCl_2$ complexes suggest that the active hydrogenation catalysts are complex systems consisting of the initial PVP–$PdCl_2$ complex and Pd(0) species stabilized within the polymer matrix. The functional groups of PVP retain the Pd(0) particles and prevent their agglomeration.

The catalytic activity of P2VP–Pd(II) and P4VP–Pd(II) complexes was investigated in the hydrogenation of allyl alcohol.

$$CH_2{=}CH\text{-}CH_2OH + H_2 \rightarrow CH_3\text{-}CH_2\text{-}CH_2OH \qquad (1)$$

Polyvinylpyridine palladium complexes promote the selective hydrogenation of allyl alcohol to propanol, providing product yields of 86–89%. Analysis of the specific rate of allyl alcohol hydrogenation revealed the following order of catalytic activity:

P4VP–Pd(0) > P2VP–Pd(0) > P4VP–Pd(II) > P2VP–Pd(II) > Pd black.

The high activity of P4VP–Pd(0) is attributed to the greater steric accessibility of palladium centers in this complex, which facilitates reduction by hydrogen or $NaBH_4$, as well as the activation of allyl alcohol and the subsequent catalytic process. The catalytic system is believed to consist of palladium species reduced to the zero-valent state and immobilized on the polymer surface, together with unreduced fragments of the poly(2-vinylpyridine) or poly(4-vinylpyridine) complexes.

The catalytic activity of PVP–$PdCl_2$ depends on the reaction conditions and the nature of the substrate (Table 3). Hydrogenation of unsaturated alcohols and aldehydes in water and ethanol showed higher activity

for PVP–$PdCl_2$ than for palladium black. Aldehydes were hydrogenated only at the double bond, while the carbonyl group remained unaffected. Hydrogenation of 2-propen-1-ol over palladium black produced 48% n-propionaldehyde due to isomerization, whereas PVP–$PdCl_2$ yielded 98–99% n-propanol. No clear correlation was observed between catalytic activity and catalyst pretreatment with reducing agents. For unsaturated alcohols, $NaBH_4$ treatment in water increased the reaction rate, while reduction in ethanol decreased catalytic activity. In contrast, for unsaturated aldehydes, $NaBH_4$ treatment in both water and ethanol lowered the hydrogenation rate.

Table 3 - Hydrogenation rates[a] of selected unsaturated oxo compounds over P2VP–$PdCl_2$ reduced with H_2 and $NaBH_4$, and over Pd black in water and ethanol[b] [4]

Hydrogenated substrate	Pd black		P2VP–$PdCl_2$			
	Water	Ethanol	Water		Ethanol	
			H_2	$NaBH_4$	H_2	$NaBH_4$
2-propen-1-ol	0.6	0.3	22.0	98.8	190.2	189.2
3-phenylpropen-2-ol-1	0.4	2.3	4.1	17.0	46.3	13.9
butene-2-al	0.7	3.2	5.3	5.0	67.9	14.6
2-phenylpropen-2-al-1	0.9	3.0	5.8	3.5	7.3	1.9

[a]Expressed in mmol H_2 (g Pd)$^{-1}$ min^{-1}.

[b]Reaction conditions: 298 K; hydrogen pressure 1 atm; substrate concentration 0.18 mol/dm.

The different behavior of alcohols and aldehydes over $NaBH_4$-reduced complexes is likely related to their activation mechanisms: alcohols are mainly activated by Pd(0), whereas aldehydes are activated by Pd(II). Hydrogenation over H_2-treated PVP–$PdCl_2$ proceeds faster in ethanol than in water, which is attributed to enhanced swelling of the polymer–metal complexes and changes in catalyst composition. Elemental analysis indicated a PVP crosslinking degree of 25–29% in the presence of Pd ions. Treatment with H_2 or $NaBH_4$ partially cleaves N–Pd bonds, forming reduced palladium species and increasing catalyst swelling, thereby improving the accessibility of active Pd sites and accelerating hydrogenation. This effect is more pronounced for small molecules, while diffusion of phenyl-containing compounds into the swollen matrix is sterically hindered. Swelling of PVP–$PdCl_2$ is significantly greater in ethanol, increasing hydrogenation rates. However, $NaBH_4$ treatment in ethanol decreases catalytic activity, likely because the higher Pd(0) content promotes agglomeration of reduced palladium species, which negatively affects activation of unsaturated compounds.

Based on the experimental results, hydrogen activation initially occurs through palladium reduction during treatment with H_2 or $NaBH_4$. Once Pd(0) species are formed, hydrogen activation mainly proceeds on Pd(0) centers, whereas unsaturated compounds can be activated on both Pd(II) and Pd(0) through π-complex formation. In swollen-gel catalytic systems, swelling facilitates access to additional active Pd sites within the polymer matrix. Flexible polymer chains suppress palladium leaching, particle growth, and agglomeration, reducing catalyst deactivation and enabling repeated reuse without significant loss of activity. Similar behavior is expected in other gel-immobilized polymer–metal catalytic systems, where activity depends on solvent swelling and the strength of metal–polymer interactions.

So, the key factor in obtaining a catalytically active $PdCl_2$–PVP complex is achieving an equilibrium palladium content in the polymer–metal complex (PMC). This can be accomplished either by prolonged aging of the complex in the mother solution or by heating the initial $PdCl_2$ and PVP solutions to 50–60 °C. An active and stable hydrogenation catalyst was obtained by reacting ethanol solutions of $PdCl_2$ and PVP at a PVP:Pd ratio of 1:1, followed by aging of the complex in the initial solution for 3 days. The catalytic activity depends on the ratio of reduced to oxidized palladium species. Pretreatment of the complex with $NaBH_4$ increased the hydrogenation rate by 5–5.5 times. The developed catalyst exhibited high activity and stability in the hydrogenation of unsaturated alcohols.

Polymer metal catalysts on oxides as a highly organized system

Catalytic activity mainly depends on the size and dispersion of metal particles. Efficient immobilization of metal catalysts, especially metal complexes, remains an important challenge. Polymer

supports often suffer from diffusion limitations and low thermal and mechanical stability; however, these drawbacks can be reduced by coating inorganic supports with functional polymers.

The new approach was developed to prepare such types of catalysts [8-9]. And based on the formation of polymer-metal complexes on the surface of oxides. The heterogeneous catalysts with uniform distribution of metal particles were prepared using linear polymer (poly-2-methyl-5-vinylpyridine) and transition metal ions (Figure 2). A suspension of oxide (0.2 g) in ethanol (5 mL) was mixed with 5 mL of an ethanol solution containing 0.011 g of PMVP (5.55 wt.% relative to the support) and stirred vigorously for 2 h. Then, 5 mL of an ethanol solution of H_2PdCl_4 containing 0.01 g of Pd (5.0 wt.% relative to the support) was added, and the mixture was stirred for at least 3 h until complete palladium binding. The resulting catalyst was aged in the mother liquor for at least 10 h, separated, washed with 50 mL of ethanol, dried, and stored in air at room temperature. The final catalyst composition (wt.%) was: Pd, 5.0; poly-2-methyl-5-vinylpyridine, 5.55; oxide support, 89.45.

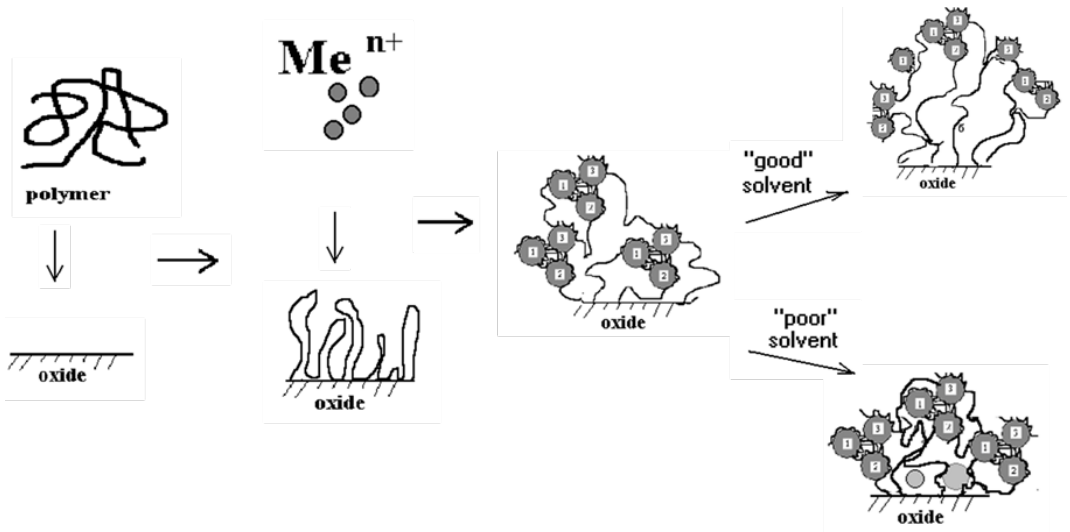

Figure 2 - Scheme for the preparation of PMC-on-oxide surface catalysts

These catalysts are characterized by small Pd particle sizes (6–8 nm) and uniform distribution over the oxide surface, as shown in the micrographs of the Pd–P2M5VP/MgO catalyst (Figure 3).

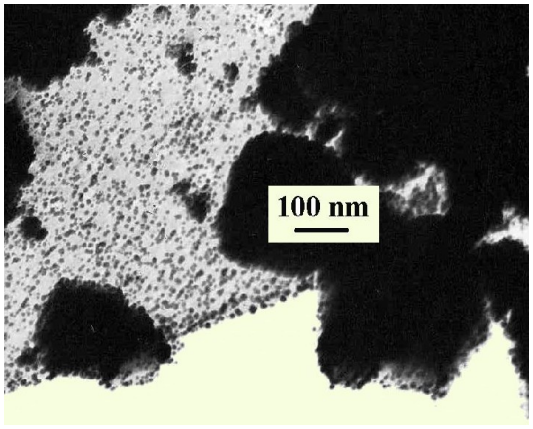

Figure 3 - Micrograph of 5% Pd–P2M5VP/MgO catalysts [9]

The catalytic activity of 5% Pd–P2M5VP catalysts supported on ZnO and MgO was investigated in the hydrogenation of the acetylenic alcohol 3,7,11-trimethyldodecin-1-ol. Hydrogenation of 3,7,11-trimethyldodecin-1-ol (TMD) was carried out in a thermostatted glass reactor under constant stirring in ethanol (0.025 L) at 50 °C and atmospheric hydrogen pressure. Before the reaction, the catalysts were treated with hydrogen for 0.5 h. To evaluate catalyst stability, TMD portions were added sequentially to the reactor.

The TMD conversion was calculated using the following equations:

$$S_{hydr.} = \frac{[3,7,11\text{-trimethyldodecene-1-ol}]}{[3,7,11\text{-trimethyldodecene-1-ol}] + [3,7,11\text{-trimethyldodecane-1-ol}]} \times 100\%$$

Hydrogenation of TMD over all prepared catalysts led to the formation of 3,7,11-trimethyldodecen-1-ol, which was subsequently hydrogenated to 3,7,11-trimethyldodecane. The hydrogenation results are summarized in Table 1. All catalysts showed nearly identical yields of olefinic alcohol, with process selectivity ranging from 82–85%.

Table 4 - Hydrogenation of TMD on palladium-supported catalysts

Catalysts	Surface area, m^2/g	Isoelectric point of oxides	Particle sizes, nm	$W10^{-5}$ mole/l sec	$S_{c=c}$, %	TON
Pd/MgO	6.8	12.1-12.7	7-10, 20-25	25.6	82	800
Pd-PMVP/MgO			5-7	21.8	85	4800
Pd/ZnO	88	7.0-9.0	30-35	16.5	85	400
Pd-PMVP/ZnO			6-8	21.4	85	6700

The results showed that the catalytic activity and selectivity were only weakly affected by the catalyst preparation method or the nature of the oxide support. In contrast, the polymer additive played a crucial role in catalyst formation and stability during hydrogenation. Comparison of turnover numbers (TON) for catalysts with and without P2M5VP demonstrated that the polymer increased catalyst stability by more than an order of magnitude (Table 4).

$PdCl_2$ forms complexes with poly(vinylpyridines) that act as active, stable, and selective hydrogenation catalysts. Their high stability is attributed to the protective effect of the polymer chains. Polymer-coated ZnO and MgO can coordinate Pd(II) ions via the pyridine nitrogen atoms of P2M5VP, resulting in a uniform Pd distribution on the oxide surfaces. This assumption is supported by electron microscopy of the Pd/MgO catalyst without polymer coating (Figure 3), which showed randomly distributed Pd particles with irregular shapes and sizes.

Thus, soluble functional polymers can be effectively used for catalyst preparation. Chemical interactions between transition-metal salts and polymer functional groups on oxide surfaces promote the uniform distribution of metal particles. Polymer chains suppress particle agglomeration and catalyst deactivation, while combining the advantages of polymer–metal catalysts, including stable activity and selectivity. An important requirement is maintaining maximum accessibility of metal particles by minimizing polymer shielding of the active surface.

Palladium-based polymer catalysts are widely used in organic synthesis, and their properties depend on the polymer composition, structure, and preparation conditions. The incorporation of polymer ligands into heterogeneous catalysts imparts characteristics typical of linear macromolecules, including swelling and sensitivity to the nature of the solvent and environmental conditions. Therefore, optimization of catalyst preparation and reaction conditions is essential. The observed phenomena can be explained by a polymer

chain sorption model that accounts for forces acting along the macromolecule. Polymer–metal interactions reduce these forces and decrease the number of polymer–surface bonds, making the process self-organizing.

References

1. Sun, J., Jiang, Y., Wang, X., Qiu, H., Li, H., Zhang, D., Chang, Y., & Liu, J. (2026). Synergistic isolated Pd1 sites and few-atom Pdn ensembles on a Au core for low-temperature acetylene semi-hydrogenation. Chemical Engineering Journal, *528*, 172411. https://doi.org/10.1016/j.cej.2025.172411

2. Nazarpour-Fard, H., Shirini, F., & Behzadi Pour, G. (2025). Heterogeneous organic reactions in the presence of poly(vinyl pyridine) and its derivatives as catalyst or reagent. Inorganic Chemistry Communications, *172*, 113691. https://doi.org/10.1016/j.inoche.2024.113691

3. Deng, X., Wang, J., Guan, N., et al. (2022). Catalysts and mechanisms for the selective heterogeneous hydrogenation of carbon–carbon triple bonds. Cell Reports Physical Science, *3*, 101017. https://doi.org/10.1016/j.xcrp.2022.101017

4. Zharmagambetova, A. K., Golodov, V. A., Saltykov, Yu. P. (1989). The study of the composition and catalytic properties of palladium(II) complexes with poly(vinylpyridine). *Journal of* Molecular Catalysis, *55*, 406–414.

5. Bekturov, E. A., Kudaibergenov, S. E., Saltybaeva S.S. (1985). Catalysts properties of polyvinylpyridine complexes of palladium. Reactive polymers, *4*, 49–53.

6. Dzhardimalieva, G. I., Zharmagambetova, A. K., Kudaibergenov, S. E., et al. (2020). Polymer-immobilized clusters and metal nanoparticles in catalysis. Kinetics and Catalysis, *61*, 198–223. https://doi.org/10.1134/S0023158420020044

7. Zharmagambetova, A. K., Mukhamedzhanova, S. G., & Bekturov, E. A. (1994). Hydrogenation catalysts based on palladium complexes with poly(vinylpyridine). Reactive Polymers, *24*(1), 17–20. https://doi.org/10.1016/0923-1137(94)90131-7

8. Zharmagambetova, A., Selenova, B., Mukhamedzhanova, S., & Kurmanbaeva, I. (2000). Design of nano-sized polymer-palladium catalysts for hydrogenation. Eurasian ChemTech *Journal, 2*, 17–20.

9. Zharmagambetova, A. K., Selenova, B., Mukhamedzhanova, S. G., et al. (2000). Supported palladium hydrogenation catalysts modified with poly-2-vinylpyridine. Russian Journal of Applied Chemistry, *73*(8), 1393–1395.

RECENT ADVANCES IN GREEN SYNTHESIS OF METAL OXIDE NANOPARTICLES USING PLANT EXTRACTS

Chinibayeva N.S.[1], Ibraimov A.B.[1], Akylbekova T.N.[1]*
*[1]Abai Kazakh National Pedagogical University, Almaty, Kazakhstan
*e-mail: t.akylbekova@abaiuniversity.edu.kz

Abstract. Green synthesis of metal oxide nanoparticles using plant extracts has emerged as a sustainable and environmentally friendly alternative to conventional chemical and physical synthesis methods. This review comprehensively examines recent advances in plant-mediated biosynthesis of various metal oxide nanoparticles, including zinc oxide, titanium dioxide (TiO_2), iron oxide (Fe_2O_3/Fe_3O_4), copper oxide, and other metal oxides. The mechanisms involving phytochemicals such as flavonoids, terpenoids, alkaloids, phenolic compounds, and saponins as reducing and stabilizing agents are discussed in detail. Characterization techniques including UV-Vis spectroscopy, X-ray diffraction, scanning electron microscopy, transmission electron microscopy, and Fourier-transform infrared spectroscopy are reviewed. Applications of green-synthesized MONPs in environmental remediation, biomedical fields, photocatalysis, antimicrobial activity, and agricultural practices are highlighted. The advantages of plant-based synthesis over microbial and chemical methods, including cost-effectiveness, scalability, and reduced environmental impact, are emphasized. Future perspectives and challenges in standardization, mechanistic understanding, and industrial translation are also addressed.

Keywords: Green synthesis, metal oxide nanoparticles, plant extracts, phytochemicals, biosynthesis, environmental remediation, biomedical applications, photocatalysis

Introduction

Nanotechnology has revolutionized materials science by enabling the manipulation of matter at the nanoscale (1-100 nm), resulting in materials with unique physicochemical properties that differ significantly from their bulk counterparts [1], [2]. Metal oxide nanoparticles have garnered considerable attention due to their versatile applications in catalysis, drug delivery, sensors, energy devices, semiconductors, food technology, agriculture, and medicine [3]. The distinctive properties of MONPs, including high surface area-to-volume ratio, enhanced reactivity, quantum confinement effects, and tunable optical and electronic characteristics, make them indispensable in modern technological applications [3], [4].

Conventional synthesis methods for MONPs, including chemical reduction, sol-gel processes, hydrothermal synthesis, and physical methods such as laser ablation and vapor-phase synthesis, often require toxic chemicals, high energy inputs, and harsh operating conditions [5], [6]. These approaches generate hazardous byproducts, pose environmental risks, and may result in nanoparticles with residual toxicity that limits their biomedical and environmental applications [5], [7]. The growing concern over environmental sustainability and the need for eco-friendly nanomaterials has driven the development of green chemistry approaches for nanoparticle synthesis [1], [8].

Green synthesis using plant extracts represents a paradigm shift in nanomaterial fabrication, offering a sustainable, cost-effective, and biocompatible alternative to traditional methods [1], [9]. Plants serve as abundant, non-toxic, and renewable sources of phytochemicals that can act as both reducing agents and stabilizing agents in nanoparticle synthesis [9], [10]. The biodiversity of plant species provides a vast library of bioactive compounds, including flavonoids, terpenoids, alkaloids, phenolic compounds, saponins, and vitamins, which can mediate the reduction of metal ions to nanoparticles and control their size, shape, and stability [8], [10].

This review provides a comprehensive analysis of recent advances in the green synthesis of metal oxide nanoparticles using plant extracts, covering synthesis mechanisms, characterization techniques, applications, and future perspectives. Special emphasis is placed on understanding the role of phytochemicals in nanoparticle formation and the advantages of plant-based synthesis over other biogenic and chemical methods.

Principles of Green Synthesis

The concept of green synthesis is rooted in the twelve principles of green chemistry, which emphasize the design of chemical processes that reduce or eliminate the use and generation of hazardous substances [7], [8]. According to Cheviron et al., three general aspects need to be considered in green synthesis: solvent medium, non-toxic reducing agents, and environmentally safe nanoparticle stabilizers [7]. Green synthesis approaches aim to minimize energy consumption, use renewable feedstocks, reduce waste generation, and design safer chemicals and processes [1], [10]. Plants are readily available, inexpensive, and do not require complex culture conditions or specialized equipment [1], [10]. The use of plant extracts eliminates the need for expensive reducing and capping agents typically used in chemical synthesis [5]. Plant-based synthesis uses water or ethanol as solvents, avoiding toxic organic solvents [1]. The process generates minimal hazardous waste and does not require high temperatures or pressures [5]. Plant extracts can be easily scaled up for industrial production, making plant-mediated synthesis suitable for large-scale commercial applications [1], [11]. Nanoparticles synthesized using plant extracts often exhibit enhanced biocompatibility and reduced toxicity, making them suitable for biomedical applications [9], [12]. Plant extracts can reduce metal ions in a much shorter time compared to fungi and bacteria, which require longer incubation periods [8], [12]. Plant extracts serve as both reducing agents and stabilizing agents, eliminating the need for additional capping agents [10].

While microbial synthesis using bacteria, fungi, and yeast has been extensively studied, plant-mediated synthesis offers several advantages [6], [10]. Microorganisms require specific culture conditions, have slower growth rates, and may produce nanoparticles with lower yields [10]. In contrast, plants can be easily cultivated, harvested, and processed, and their extracts contain a diverse array of phytochemicals that can be tailored for specific nanoparticle synthesis requirements [1], [8]. Additionally, handling and controlling plant material is easier compared to other biological systems [13].

Phytochemicals as Reducing and Stabilizing Agents

The efficiency of plant-mediated synthesis of metal oxide nanoparticles is primarily attributed to the diverse range of phytochemicals naturally present in plant extracts, which function as reducing, stabilizing, and capping agents during nanoparticle formation [14]. These bioactive compounds include flavonoids, terpenoids, alkaloids, phenolic compounds, tannins, saponins, vitamins, proteins, polysaccharides, and

various secondary metabolites that collectively facilitate the conversion of metal ions into stable nanoscale materials[15]. Among these constituents, flavonoids are considered particularly important due to their strong electron-donating ability arising from multiple hydroxyl and carbonyl functional groups, which enable efficient reduction of metal ions [16] . In addition to their reducing capacity, flavonoids contribute to nanoparticle stabilization [17] and are known for their antioxidant, antimicrobial, anticancer, antiviral, and hepatoprotective properties, which may enhance the biological functionality of the synthesized nanoparticles[18]. Phenolic compounds and tannins also play a major role in nanoparticle synthesis through electron transfer mechanisms and surface adsorption, thereby preventing particle aggregation and improving colloidal stability [19] . Similarly, terpenoids and alkaloids participate in the bioreduction process and can significantly influence nanoparticle morphology, crystallinity, and surface characteristics[20].

The synergistic interaction of these phytochemicals strongly affects the physicochemical properties, yield, and stability of the synthesized nanoparticles [21] . Saponins contribute to stabilization by modifying surface interactions and dispersion behavior[22], while water-soluble vitamins, coenzymes, amino acids, and other metabolites further support reduction and nucleation processes[23]. The composition and concentration of phytochemicals vary considerably among plant species, extraction methods, plant organs, and environmental conditions, leading to differences in nanoparticle size, shape, and biological activity [24] . Consequently, plant extracts represent highly versatile and environmentally sustainable nanofactories capable of producing nanoparticles with tunable properties suitable for biomedical, catalytic, environmental, and pharmaceutical applications [25] . Figure 1 illustrates the major classes of phytochemicals involved in plant-mediated synthesis of metal oxide nanoparticles and their respective roles in reduction, stabilization, capping, and enhancement of nanoparticle properties.

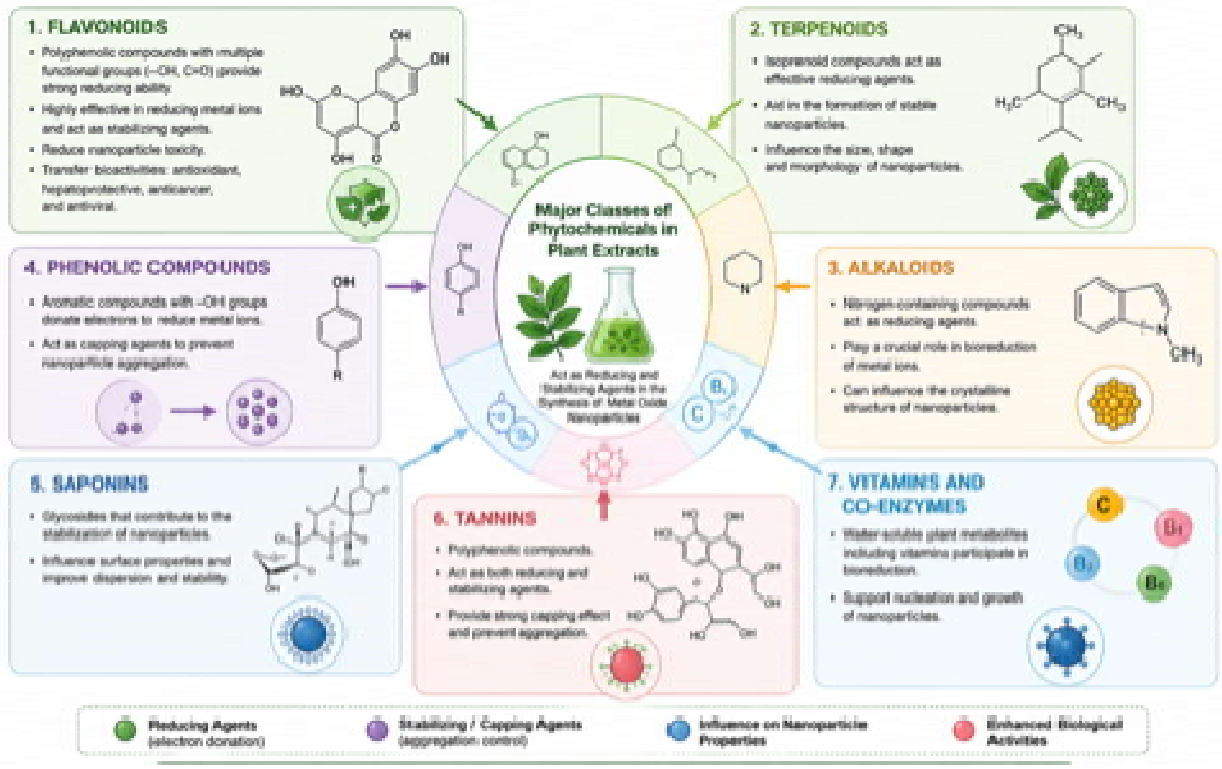

Figure 1 - Major Classes of Phytochemicals Involved in Green Synthesis of Metal Oxide Nanoparticles

Mechanism of Nanoparticle Formation

The green synthesis of nanoparticles using plant extracts is governed by a complex sequence of physicochemical interactions involving the reduction, nucleation, growth, and stabilization of metal species by naturally occurring phytochemicals. Plant-derived biomolecules such as flavonoids, phenolic acids, terpenoids, alkaloids, proteins, polysaccharides, and other secondary metabolites play a central role throughout the synthesis process. Initially, metal ions interact with functional groups present in these compounds through coordination and electrostatic interactions, resulting in the formation of intermediate

metal–phytochemical complexes that facilitate the reduction process. Subsequently, reducing agents present in the extract donate electrons to the metal ions, converting them into their reduced metallic or metal oxide forms and initiating the formation of nanoscale nuclei. These nuclei act as active centers for further nanoparticle growth through continuous deposition and aggregation of reduced metal species. As the reaction progresses, biomolecules from the plant extract adsorb onto the nanoparticle surface, functioning simultaneously as stabilizing and capping agents that inhibit excessive aggregation, regulate particle growth, and improve colloidal stability. Consequently, the size, morphology, crystallinity, and dispersion of the synthesized nanoparticles are strongly influenced by the nature and concentration of phytochemicals present in the extract [12], [26] . Figure 2 schematically illustrates the mechanism of plant-mediated synthesis of metal oxide nanoparticles, including phytochemical-assisted reduction of metal ions, nucleation, nanoparticle growth, and stabilization through capping by bioactive compounds.

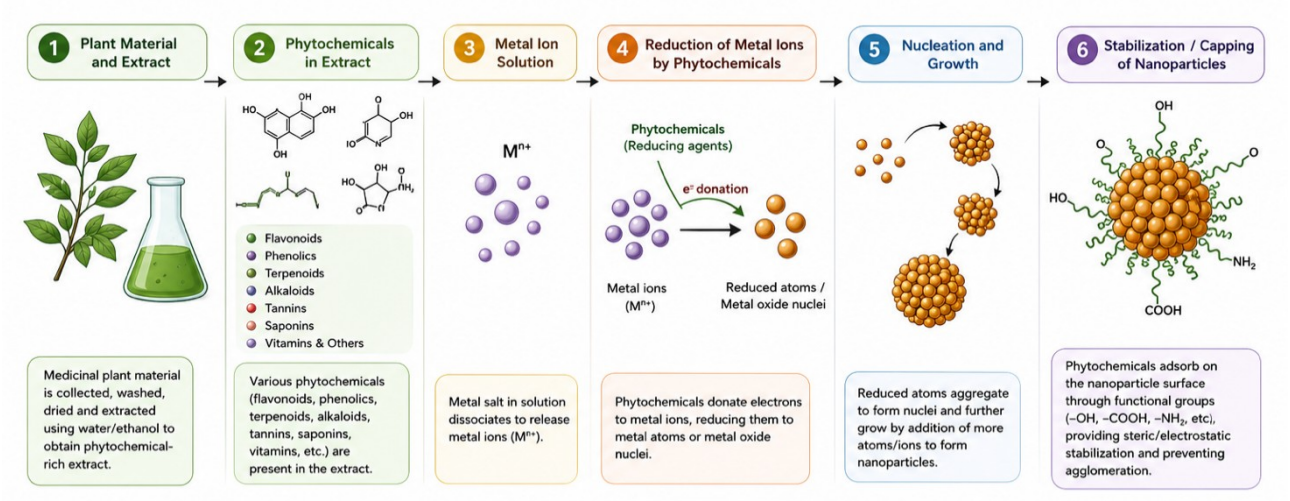

Figure 2 - Mechanism of Green Synthesis of Metal Oxide Nanoparticles Using Plant Extracts.

The efficiency and characteristics of green nanoparticle synthesis are also highly dependent on reaction parameters, including pH, temperature, reaction time, metal precursor concentration, and extract composition[27]. Variations in pH can significantly alter the ionization state of phytochemicals and influence reduction kinetics, nucleation rate, and nanoparticle stability [27] . Similarly, temperature affects reaction kinetics and particle crystallization[27], while the concentration of plant extract determines the availability of reducing and stabilizing compounds [27] . Studies have shown that biopolymers such as lignin may simultaneously function as reducing and stabilizing agents, with their concentration directly affects nanoparticle size distribution and dispersion behavior [28] . In summary, the synergistic interaction between phytochemical constituents and reaction conditions governs the formation mechanism, yield, structural properties, and long-term stability of green-synthesized nanoparticles, making plant-mediated synthesis an environmentally friendly and highly tunable approach for nanomaterial production.

Green Synthesis of Specific Metal Oxide Nanoparticles

Zinc Oxide Nanoparticles

Zinc oxide nanoparticles are among the most extensively studied metal oxides due to their diverse applications in antibacterial, antifungal, anticancer, antidiabetic treatments, drug delivery, and agricultural technologies [4], [13] . Green-synthesized ZnO NPs show potent antibacterial effects at very low concentrations compared to chemically synthesized ZnO NPs [13] . Various plant leaf extracts have been used to prepare ZnO NPs, including coriander, crown flower, Copper leaf, China rose, green tea, and aloe leaf broth extract [12] . Other plants include Azadirachta indica, Aloe barbadensis Miller, Moringa oleifera, Artocarpus heterophyllus (jackfruit), and Syzygium cumini [2], [4], [29] . Madan et al. followed a low-temperature solution combustion route, employing Azadirachta indica leaf extract as a template to synthesize multifunctional hexagonal wurtzite-structured ZnO nanoparticles with various morphologies [2] . Ali et al. prepared ZnO nanoparticles using the reducing and capping potential of Aloe barbadensis Miller leaf extract [2] . Vidya et al. demonstrated green synthesis of ZnO NPs utilizing Artocarpus heterophyllus leaf

(jackfruit) extract, producing hexagonal wurtzite-like shaped particles with a size of 15–25 nm [4] . The PXRD patterns confirmed the hexagonal phase of ZnO with wurtzite structure. SEM and TEM analysis revealed rectangular flake-like structures for chemical ZnO whereas green ZnO NPs exhibited spherical structures [13] . The crystalline structure of ZnO NPs was confirmed by XRD analysis and Raman investigation [4] . ZnO NPs synthesized using plant extracts have demonstrated significant antibacterial activity against various bacterial strains [2], [29] . Green ZnO NPs exhibited better antibacterial and antifungal activities in addition to superior photocatalytic behavior [13]. The antibacterial studies indicated that ZnONPs had significant antibacterial activity against K. aerogenes and S. aureus, but not against E. coli and P. aeruginosa [2]. ZnO NPs have shown high photodegradation efficiency (>80% in 1 h) against Rose Bengal dye [4].

Titanium Dioxide Nanoparticles (TiO_2 NPs)

Titanium dioxide nanoparticles are widely used in personal care products, catalysis, and solar cells[30]. Green synthesis methods for TiO_2 NPs have been developed to avoid the environmental impacts of conventional synthesis methods [31] . Various plant extracts have been employed for TiO_2 NP synthesis, though specific examples in the literature are less extensive compared to ZnO NPs[32]. TiO_2 nanoparticles were generally spherically agglomerated in the 10-30 nm range during TEM investigation, and SAED investigation revealed a crystalline form [33].

Iron Oxide Nanoparticles (Fe_2O_3/Fe_3O_4 NPs)

Iron oxide nanoparticles have great potential for water pollution remediation applications due to their ability to efficiently extract pollutants from solutions using a magnetic field. Green synthesis of iron oxide nanorods mediated by polyphenols present in Omani mango tree leaves has been carried out [2] . Researchers successfully applied the as-synthesized material in heavy crude oil viscosity treatment [34].

Copper Oxide Nanoparticles

Copper oxide nanoparticles have been synthesized using various plant extracts and have shown promising applications in catalysis and antimicrobial activity. Thakur et al. developed technology for manufacturing barium ferrite nanoparticles from Acorus calamus rhizome extract and examined their antifungal activity against pathogenic fungi affecting multiple plant species [10]. Madhukara et al. produced zinc ferrite nanoparticles from Limonia acidissima using the green synthesis method, and the resulting nanoparticles demonstrated excellent photodegradation of Evans blue and methylene blue when exposed to visible light [10]. Table 1 summarizes representative examples of plant-mediated synthesis of metal oxide nanoparticles and their major applications reported in recent studies. Various plant extracts rich in phytochemicals such as flavonoids, phenolics, terpenoids, and alkaloids have been successfully utilized as reducing and stabilizing agents for the synthesis of nanoparticles including ZnO, TiO_2, CuO, Fe_3O_4, and CeO_2. The synthesized nanoparticles exhibit diverse physicochemical properties and demonstrate promising applications in biomedical, environmental, catalytic, agricultural, and sensing fields. The data presented in Table 1 highlight the versatility, eco-friendliness, and functional potential of green-synthesized metal oxide nanoparticles for advanced technological and biomedical applications.

Table 1 - Plant-Mediated Synthesis of Metal Oxide Nanoparticles and Their Applications

Plant Source	Nanoparticle	Major Phytochemicals	Particle Size	Main Application
Artemisia annua	ZnO	Flavonoids, phenolics	20–50 nm	Antibacterial
Moringa oleifera	CuO	Terpenoids, tannins	15–40 nm	Photocatalysis
Azadirachta indica	Fe_3O_4	Alkaloids, flavonoids	10–30 nm	Drug delivery
Camellia sinensis	TiO_2	Polyphenols	25–60 nm	Dye degradation

Characterization Techniques

Comprehensive characterization of green-synthesized metal oxide nanoparticles is essential to understand their physicochemical properties and correlate them with their applications [33], [35] . The following techniques are commonly employed:

UV-Visible Spectroscopy

UV-Vis spectroscopy is the primary technique used for the characterization of nanoparticles, providing information about particle aggregation and optical properties [35]. It is employed to analyze the dimensions and configurations of nanoparticles in a water-based solution [33]. Typically, wavelengths in the

range of 300 to 800 nm are utilized to characterize nanoparticles with sizes ranging from approximately 2-100 nm [33]. Previous research findings have shown that the absorption of wavelengths of 200-800 nm was suitable for classifying nanoparticles with a size range of 2-100 nm [36].

X-Ray Diffraction

X-ray diffraction is a valuable technique for gaining insights into the structural aspects, size, and phase composition of metallic nanoparticles [33]. By directing X-rays at nanomaterials, the diffraction pattern that results can be compared to reference patterns to determine structural features [33] . XRD provides information about the different phases of a crystalline material and provides nanoparticle dimensions [35]. It can analyze the atomic structures of materials, and the qualitative and quantitative composition of materials can be determined with this technology [36]. Crystalline nanoparticle size and structure were identified and verified by XRD analysis [36] . To analyze the particle dimensions of nanoparticles from XRD data, the Debye-Scherrer formula is applied by measuring the width of the Bragg reflection peak [36], [37].

Scanning Electron Microscopy

Scanning electron microscopy analyzes the surface morphology of nanoparticles through the use of a focused electron beam [35], [38]. It offers fine-grained visuals of the size, shape, texture, and dispersion of the nanoparticle [38]. SEM can be used to characterize nanoparticle distribution, morphology, size, and form of synthesized nanoparticles [36]. The SEM study measured changes in morphological structure both before and after treatment [36]. According to earlier research, observable changes in cell shape and the presence of nanoparticle perforations in the cell wall are used as indicators of the antibacterial activity of nanoparticles [36]. Energy dispersive X-ray spectroscopy, which is connected to the SEM equipment, is another method for obtaining information on elemental composition [38].

Transmission Electron Microscopy

Transmission electron microscopy is the most efficient and widely used technique for the characterization of nanoparticles [35] . TEM images provide insights into the size and aggregation of nanoparticles, and single nanoparticles can be studied by TEM while SEM cannot resolve them [35]. TEM is typically used to describe the morphology and size of nanoparticles [33] . Additionally, the distribution of nanoparticles in a material TEM can reveal [38]. Green-synthesized carbon nanotubes were entirely wrapped in polyaniline layers for TEM and SEM examination [33].

Fourier-Transform Infrared Spectroscopy

FTIR spectra reveal the functional groups present on the nanoparticle surface during its synthesis [35]. This technique is crucial for identifying the phytochemicals responsible for reduction and stabilization of nanoparticles [37]. FTIR is one of the most frequent methods used to explore the structural characteristics of nanomaterials, along with XRD, energy dispersive X-ray, XPS, and Zeta size analysis [37].

Dynamic Light Scattering

Dynamic light scattering measures the size distribution of suspended nanoparticles by analyzing the light scattering resulting from the Brownian motion of the particles [38]. This approach provides information regarding hydrodynamic size and polydispersity, which is very helpful when researching nanoparticles in colloidal fluids [38].

Morphological and Elemental Characterization

The size, shape, and spatial distribution of nanoparticles are primarily assessed through electron microscopy [39]. SEM provides detailed topographical images of the surface features, texture, and degree of agglomeration [36], [38] . When coupled with Energy Dispersive X-ray spectroscopy, it allows for the quantitative and qualitative determination of elemental composition, ensuring that the target metal oxide is the dominant phase and identifying any residual biological elements (such as C, N, or O from the extract) that contribute to the capping layer [40], [41] . TEM is critical for high-resolution imaging of individual nanoparticles, enabling the observation of their internal lattice structure and precise shape (e.g., spherical, hexagonal, or rod-like) [35], [42]. Furthermore, Selected Area Electron Diffraction patterns obtained during TEM analysis provide independent verification of the crystalline or polycrystalline nature of the particles, often showing bright concentric rings that correspond to specific lattice planes [33].

Physical Stability and Surface Area

DLS measures the hydrodynamic size of the particles in a colloidal suspension, which is often larger than the "core" size measured by TEM due to the presence of the solvated capping layer [38], [43]. The Zeta potential indicates the surface charge and serves as a predictor of colloidal stability; high absolute values (typically > ±30 mV) suggest strong electrostatic repulsion, preventing sedimentation and aggregation [38],

[43]. Brunauer-Emmett-Teller (BET) measurements are used to determine the specific surface area and pore size distribution [6]. For metal oxides used in catalysis or environmental remediation, a high SSA is critical, as it provides a greater number of active sites for adsorption or redox reactions [44] , [45] . Other characterization techniques include X-ray photoelectron spectroscopy, which is commonly used to establish the actual elemental ratio and bonding type of the elements in nanoparticle materials [46] , and atomic absorption spectroscopy [47].

Factors Affecting Green Synthesis

Several parameters influence the green synthesis of metal oxide nanoparticles using plant extracts [8], [12]:

Plant Extract Parameters

Different plants comprise varying concentration levels of phytochemicals, which affect nanoparticle synthesis [8], [12]. The composition of the plant leaf extract is an important factor in nanoparticle synthesis [8] . The concentration of phytochemicals in the plant leaf extract plays a significant role in nanoparticle production [12]. Higher concentrations generally lead to faster reduction and smaller particle sizes[48]. The method of extract preparation (e.g., boiling, maceration, solvent extraction) affects the types and concentrations of phytochemicals extracted [49].

Reaction Conditions

The concentration of the metal precursor influences nanoparticle size, yield, and morphology [8], [12]. Higher concentrations may lead to larger particles or aggregation [50] . The pH of the reaction medium significantly affects nanoparticle formation [10], [12] . The mechanism of nanoparticle production using lignin notably depends on pH, with lignin concentration affecting the size and dispersion of silver nanoparticles [10] . Reaction temperature affects the kinetics of nanoparticle formation and can influence particle size and crystallinity [8], [12]. The duration of the reaction affects nanoparticle size and yield [8]. Plant extracts can reduce metal ions in a much shorter time compared to fungi and bacteria [8], [12] . The method of mixing (stirring, sonication, etc.) can affect nanoparticle uniformity and size distribution.

Applications of Green-Synthesized Metal Oxide Nanoparticles

Environmental Remediation

Green-synthesized metal oxide nanoparticles have shown pivotal roles in several environmental applications such as nano-adsorbents, nano-membranes, photocatalysts, and disinfection of microbial wastewater [2], [5].

Bio-synthesized metal oxide nanoparticles have triggered huge global research interest owing to their advantageous properties and various environmental remediation and water treatment applications [3] . They offer significant advantages in various industries, attributable to their heightened physicochemical, optical, mechanical, and electronic attributes [3] . Environmentally friendly nanoparticles are widely used to treat environmental pollutants, including the removal of heavy metals [5]. Green-synthesized MONPs are used for photocatalytic degradation of organic pollutants [5]. ZnO NPs have shown high photodegradation efficiency (>80% in 1 h) against Rose Bengal dye [4] . The photocatalytic efficiency of 98% for Acid Red 88 dye degradation was recorded for ZnO NPs [29] . The synthesized Cu/ZnO composite nanomaterial exhibited excellent catalytic activity in degrading methylene blue and congo red dyes in their aqueous solutions in the presence of $NaBH_4$ [2] . Zinc ferrite nanoparticles demonstrated excellent photodegradation of Evans blue and methylene blue when exposed to visible light [10].

Biomedical Applications

Metal oxide nanoparticles have found their inevitable place in the field of nanotechnology due to their versatile applications in drug delivery, sensors, and medicine [6], [11] . ZnO NPs have extraordinary antibacterial properties due to their expanded specific surface area, as the reduced particle size leads to enhanced surface reactivity [13]. Green-synthesized ZnO NPs show potent antibacterial effects at very low concentrations [13] . Green ZnO NPs demonstrated antibacterial activity against Pseudomonas aeruginosa, Klebsiella oxytoca, and Escherichia coli [29]. The antibacterial activity of ZnO NPs was investigated against three bacterial strains: E. coli, Salmonella paratyphi, and Staphylococcus aureus [10] . The percentage of inhibition of mycelial growth was observed during antifungal testing of ZnO NPs [29] . ZnO NPs have diverse applications in fields such as anticancer treatments[10]. Flavonoids have anticancer properties, which can be transferred to synthesized nanoparticles [9] . Metal oxide nanoparticles are used in drug delivery applications [7], [11] . Zinc oxide nanoparticles derived from Ficus microcarpa leaf extracts exhibited high

larvicidal efficacy against mosquitoes and demonstrated antibacterial properties [10]. Green synthesis metals and their oxide nanoparticles show therapeutic efficiency in periodontitis [12].

Photocatalytic Applications

When excited by light with an energy greater than the bandgap of ZnO, electrons from the valence band are excited to the conduction band to form photogenerated electrons in the CB and photogenerated holes in the VB [51]. These photogenerated electrons and holes migrate to the surface of ZnO to react with H_2O and O_2 to generate $O_2^{\bullet-}$ and •OH radicals, which oxidize organic substances [51]. ZnO NPs are an effective futuristic water purification material [52]. ZnO NPs can exhibit photo-oxidizing and photocatalytic effects on chemical and biological species [51] . Green ZnO NPs exhibited superior photocatalytic behavior [29]. Methylene Blue decolorization under sunlight was examined to determine the photocatalytic activity of the generated ZnO NPs, which completed in 90 min[4]. ZnO NPs were used to generate hydrogen via photocatalysis [4] . The development of this field has progressed from simple exploratory studies involving plant extracts toward highly optimized, multifunctional, and application-oriented nanomaterials. Significant improvements in synthesis control, nanoparticle stability, characterization techniques, and large-scale production have enabled the expansion of green-synthesized nanoparticles into biomedical, environmental, catalytic, agricultural, and energy-related applications. Recent trends further emphasize sustainable nanotechnology, multifunctional nanoparticle systems, and the integration of artificial intelligence and smart technologies for process optimization and advanced material design, indicating the growing scientific and technological importance of green nanomaterials in future research and industrial applications. Figure 3 presents the overall evolution of green nanotechnology and highlights the major advances achieved in plant-mediated synthesis of metal oxide nanoparticles over the past decades.

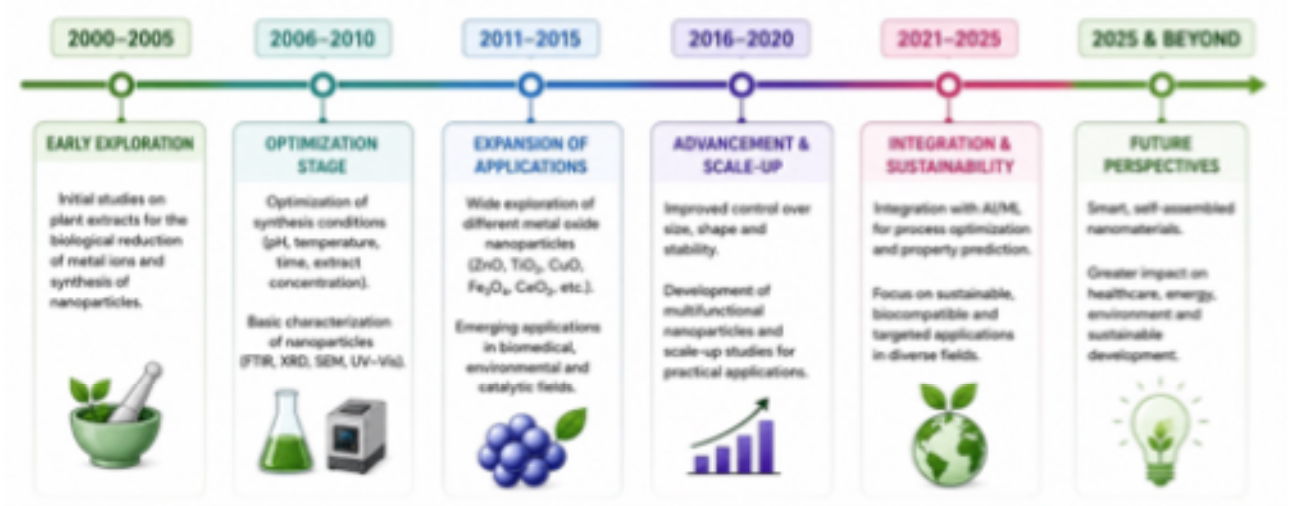

Figure 3 - Evolution and Development Trends of Green Nanotechnology in Plant-Mediated Metal Oxide Nanoparticle Synthesis

Challenges and Limitations

Despite the numerous advantages of green synthesis of metal oxide nanoparticles using plant extracts, several challenges and limitations need to be addressed:

Mechanistic Understanding

The definite role of phytochemicals in nanoparticle synthesis has not been fully determined [53] . Although the feasibility of controlling the size and shape of nanoparticles by variation in reaction conditions has been demonstrated in many studies, the actual mechanism by which plant constituents contribute to the synthetic process remains fully unknown [1] . More research is needed to elucidate the precise molecular mechanisms involved in nanoparticle formation.

Standardization and Reproducibility

Specific conditions should be considered for the preparation of nanoparticles from different plant species [38] . Variations in plant composition due to seasonal, geographical, and environmental factors can lead to batch-to-batch variability in nanoparticle synthesis [54]. Standardization of protocols is essential for reproducible results.

Yield and Scalability

While plant-mediated synthesis is considered scalable, achieving high yields with consistent quality remains a challenge [7], [12] . The mass production of atomically precise nanoparticles requires highly reactive substances and/or energy-consuming procedures, which are not considered environmentally friendly [7]. Optimization of synthesis parameters is needed for industrial-scale production.

Purification and Separation

Separation of nanoparticles from plant extracts and purification to remove residual phytochemicals can be challenging [1], [55] . Efficient purification methods need to be developed to ensure nanoparticle purity for specific applications.

Characterization of Phytochemical-Nanoparticle Interactions

Understanding the interactions between phytochemicals and nanoparticle surfaces is crucial for controlling nanoparticle properties[56],[10] . Advanced characterization techniques are needed to study these interactions at the molecular level.

Toxicity Assessment

While green-synthesized nanoparticles are generally considered less toxic, comprehensive toxicity assessment is necessary for biomedical and environmental applications [3], [5] . Long-term environmental and health impacts need to be studied.

Conclusion

Green synthesis of metal oxide nanoparticles using plant extracts has emerged as a sustainable and environmentally friendly alternative to conventional chemical and physical synthesis methods. The use of plant extracts as precipitating agents for the preparation of metal oxides eliminates the use of hazardous chemicals. Phytochemicals, which are active substances obtained from plants, serve as reducing and stabilizing agents in the ecologically benign manufacturing of nanoparticles. This review comprehensively examines recent advances in the green synthesis of various metal oxide nanoparticles, including ZnO, TiO_2, Fe_2O_3, CuO, and others, using diverse plant extracts. The mechanisms involving phytochemicals such as flavonoids, terpenoids, alkaloids, phenolic compounds, and saponins have been discussed in detail. Characterization techniques including UV-Vis spectroscopy, XRD, SEM, TEM, and FTIR have been reviewed.

The applications of green-synthesized MONPs in environmental remediation, biomedical fields, photocatalysis, antimicrobial activity, agricultural practices, energy, food, and sensing applications have been highlighted. Green-synthesized nanoparticles often exhibit enhanced biocompatibility, reduced toxicity, and superior performance compared to chemically synthesized nanoparticles. Plant-mediated synthesis offers numerous advantages including cost-effectiveness, scalability, environmental friendliness, and biocompatibility. However, challenges related to mechanistic understanding, standardization, yield, purification, and toxicity assessment need to be addressed for wider adoption and industrial translation.

Future research should focus on elucidating precise mechanisms, standardizing protocols, developing hybrid nanoparticles, exploring novel applications, contributing to the circular bioeconomy, employing computational modeling, facilitating industrial translation, and developing regulatory frameworks. With continued research and development, green synthesis using plant extracts has the potential to revolutionize the production of metal oxide nanoparticles and contribute to sustainable nanotechnology.

References:

1. Khandel, P., Yadaw, R. K., Soni, D. K., Kanwar, L., & Shahi, S. K. (2018). Biogenesis of metal nanoparticles and their pharmacological applications: Present status and application prospects. Journal of Nanostructure in Chemistry, 8(3), 217–254. https://doi.org/10.1007/s40097-018-0267-4

2. Gebre, S. H., & Sendeku, M. G. (2019). New frontiers in the biosynthesis of metal oxide nanoparticles and their environmental applications: An overview. SN Applied Sciences, 1(8). https://doi.org/10.1007/s42452-019-0931-4

3. Aigbe, U. O., & Osibote, O. A. (2024). Green synthesis of metal oxide nanoparticles, and their various applications. Journal of Hazardous Materials Advances, 13, 100401. https://doi.org/10.1016/j.hazadv.2024.100401

4. Hassaan, M. A., El-Nemr, M. A., Elkatory, M. R., Ragab, S., Niculescu, V., & Nemr, A. E. (2023). Principles of photocatalysts and their different applications: A review. Topics in Current Chemistry, 381(6). https://doi.org/10.1007/s41061-023-00444-7

5. Ashour, M., Mansour, A. T., Abdelwahab, A. M., & Alprol, A. E. (2023). Metal oxide nanoparticles' green synthesis by plants: Prospects in phyto- and bioremediation and photocatalytic degradation of organic pollutants. Processes, 11(12), 3356. https://doi.org/10.3390/pr11123356

6. Singh, K. R., Nayak, V., Singh, J., Singh, A. K., & Singh, R. P. (2021). Potentialities of bioinspired metal and metal oxide nanoparticles in biomedical sciences. RSC Advances, 11(40), 24722–24746. https://doi.org/10.1039/d1ra04273d

7. Peralta-Videa, J. R., et al. (2016). Plant-based green synthesis of metallic nanoparticles: Scientific curiosity or a realistic alternative to chemical synthesis? Nanotechnology for Environmental Engineering, 1(1). https://doi.org/10.1007/s41204-016-0004-5

8. Singh, J., Dutta, T., Kim, K., Rawat, M., Samddar, P., & Kumar, P. (2018). 'Green' synthesis of metals and their oxide nanoparticles: Applications for environmental remediation. Journal of Nanobiotechnology, 16(1). https://doi.org/10.1186/s12951-018-0408-4

9. Shafey, A. M. E. (2020). Green synthesis of metal and metal oxide nanoparticles from plant leaf extracts and their applications: A review. Green Processing and Synthesis, 9(1), 304–339. https://doi.org/10.1515/gps-2020-0031

10. Osman, A. I., et al. (2024). Synthesis of green nanoparticles for energy, biomedical, environmental, agricultural, and food applications: A review. Environmental Chemistry Letters, 22(2), 841–887. https://doi.org/10.1007/s10311-023-01682-3

11. Parveen, S., et al. (2025). Green synthesis of metal oxide nanoparticles via plant extracts for biological applications: A review. Trends in Sciences, 22(6), 9592. https://doi.org/10.48048/tis.2025.9592

12. Kiarashi, M., et al. (2024). Spotlight on therapeutic efficiency of green synthesis metals and their oxide nanoparticles in periodontitis. Journal of Nanobiotechnology, 22(1). https://doi.org/10.1186/s12951-023-02284-5

13. Kahsay, M. H., Tadesse, A., RamaDevi, D., Belachew, N., & Basavaiah, K. (2019). Green synthesis of zinc oxide nanostructures and investigation of their photocatalytic and bactericidal applications. RSC Advances, 9(63), 36967–36981. https://doi.org/10.1039/c9ra07630a

14. Krishna, P. G., et al. (2022). Photocatalytic activity induced by metal nanoparticles synthesized by sustainable approaches: A comprehensive review. Frontiers in Chemistry, 10. https://doi.org/10.3389/fchem.2022.917831

15. Kaur, J., Soni, H., Acevedo, R., & Verma, M. (2024). Green synthesis of silver nanoparticles and their antimicrobial applications. E3S Web of Conferences, 509, 1017. https://doi.org/10.1051/e3sconf/202450901017

16. Arora, S. K., et al. (2021). Greener approach to metallic nanoparticles: A review. Nature Environment and Pollution Technology, 20(2). https://doi.org/10.46488/nept.2021.v20i02.004

17. Darnis, D. S., Haris, M. S., Taher, M., & Khotib, J. (2022). Natural products-based metallic nanoparticles as antimicrobial agents. Frontiers in Pharmacology, 13. https://doi.org/10.3389/fphar.2022.895616

18. Dwivedi, K., et al. (2023). Emergence of nano-based formulations for effective delivery of flavonoids against topical infectious disorders. Gels, 9(8), 671. https://doi.org/10.3390/gels9080671

19. Gangwar, C., Yaseen, B., Kumar, I., Singh, N. K., & Naik, R. M. (2021). Growth kinetic study of tannic acid mediated monodispersed silver nanoparticles synthesized by chemical reduction method and its characterization. ACS Omega, 6(34), 22344–22356. https://doi.org/10.1021/acsomega.1c03100

20. Muhaimin, M., Chaerunisaa, A. Y., Rostinawati, T., Amalia, E., Hazrina, A., & Nurhasanah, S. (2023). A review on nanoparticles of Moringa oleifera extract: Preparation, characterization, and activity. International Journal of Applied Pharmaceutics, 43–51. https://doi.org/10.22159/ijap.2023v15i4.47709

21. El-Fitiany, R. A., et al. (2025). Secret elixirs of nature: Extract type shapes the phytochemical-mediated synthesis and anticancer potential of ZnO and Fe_2O_3 nanoparticles from Salvadora persica. Scientific Reports, 15(1). https://doi.org/10.1038/s41598-025-20577-7

22. Morales-Juárez, L. R., Duran-Casco, M. de L. G., Melo, M. A. M., Rodríguez-Victoria, Á. P., Sanchez, O. F., & Vázquez-Cuchillo, O. (2024). Easy synthesis of Au nanoparticles at low temperature using Saponin quillaja sp. and its photocatalytic activity. Materials Letters, 363, 136237. https://doi.org/10.1016/j.matlet.2024.136237

23. Kulkarni, D., et al. (2023). Biofabrication of nanoparticles: Sources, synthesis, and biomedical applications. Frontiers in Bioengineering and Biotechnology, 11. https://doi.org/10.3389/fbioe.2023.1159193

24. Rocha, M. B. da C., Araújo, T. R. de, Medeiros, R. L. B. A., Oliveira, M. M., & Figueredo, G. P. de. (2021). Recent advances (2016–2020) in green synthesis of metal oxide nanoparticles: An overview. Research, Society and Development, 10(16). https://doi.org/10.33448/rsd-v10i16.23406

25. Khan, H., Piccolella, S., & Pacifico, S. (2025). Harnessing plant extracts for green nanoparticle synthesis: Toward a sustainable future. Materials Today Sustainability, 31, 101195. https://doi.org/10.1016/j.mtsust.2025.101195

26. Vanitha, G., Manikandan, R., Sathiyamoorthi, K., & Dhinakaran, B. (2022). Review on green synthesis of nanoparticles using various strong electrolytic metal solutions mediated by various plant parts. Journal of Nanoscience and Technology, 8(2), 960–966. https://doi.org/10.30799/jnst.334.22080201

27. Alam, F., et al. (2025). Eco-compatible synthesis of metal nanoparticles: Influencing parameters, characterization, advancement and applications. Asian Journal of Chemistry, 37(11), 2617–2630. https://doi.org/10.14233/ajchem.2025.34459

28. Lizundia, E., et al. (2021). Multifunctional lignin-based nanocomposites and nanohybrids. Green Chemistry, 23(18), 6698–6760. https://doi.org/10.1039/d1gc01684a

29. Raj, N. B., et al. (2021). Harnessing ZnO nanoparticles for antimicrobial and photocatalytic activities. Journal of Photochemistry and Photobiology, 6, 100021. https://doi.org/10.1016/j.jpap.2021.100021

30. Pradhan, A., Fernandes, M., Martins, P. M., Pascoal, C., Lanceros-Méndez, S., & Cássio, F. (2021). Can photocatalytic and magnetic nanoparticles be a threat to aquatic detrital food webs? The Science of the Total Environment, 769, 144576. https://doi.org/10.1016/j.scitotenv.2020.144576

31. Rodríguez-Rojas, M. del P., Bustos-Terrones, V., Díaz-Cárdenas, M. Y., Vázquez-Vélez, E., & Martínez, H. (2024). Life cycle assessment of green synthesis of TiO_2 nanoparticles vs. chemical synthesis. Sustainability, 16(17), 7751. https://doi.org/10.3390/su16177751

32. Kushwah, K. S., & Verma, D. K. (2021). Biological synthesis of metallic nanoparticles from different plant species. In IntechOpen eBooks. https://doi.org/10.5772/intechopen.101355

33. Mawthoh, A. B. T., Seram, D., & Watt, H. J. (2023). Green synthesized plant-based nanotechnology: Cutting edge innovation fostering sustainability and revolutionizing agriculture. E3S Web of Conferences, 453, 1018. https://doi.org/10.1051/e3sconf/202345301018

34. Kumar, B., et al. (2023). Iron ores and iron oxides: New perspectives. IntechOpen. https://doi.org/10.5772/intechopen.103994

35. Kumar, D., & Seth, C. S. (2021). Green-synthesis, characterization, and applications of nanoparticles (NPs): A mini review. International Journal of Plant and Environment, 7(1), 91–95. https://doi.org/10.18811/ijpen.v7i01.11

36. Jha, S. K., & Jha, A. (2024). Sustainable utilization of renewable plant-based material for the green synthesis of metal nanoparticles. In IntechOpen eBooks. https://doi.org/10.5772/intechopen.112672

37. Salem, S. S. (2023). A mini review on green nanotechnology and its development in biological effects. Archives of Microbiology, 205(4). https://doi.org/10.1007/s00203-023-03467-2

38. Ilavenil, K. K., Senthilkumar, V., & Kasthuri, A. (2025). Green synthesis of metal nanoparticles from three medicinal plants: A review of environmental and health applications. Discover Catalysis, 2(1). https://doi.org/10.1007/s44344-025-00007-6

39. Joudeh, N., & Linke, D. (2022). Nanoparticle classification, physicochemical properties, characterization, and applications: A comprehensive review for biologists. Journal of Nanobiotechnology, 20(1). https://doi.org/10.1186/s12951-022-01477-8

40. Nguyen, T. H. A., et al. (2021). Novel biogenic silver and gold nanoparticles for multifunctional applications: Green synthesis, catalytic and antibacterial activity, and colorimetric detection of Fe(III) ions. Chemosphere, 287, 132271. https://doi.org/10.1016/j.chemosphere.2021.132271

41. Koliyote, S., & Shaji, J. (2023). A recent review on synthesis, characterization and activities of gold nanoparticles using plant extracts. Indian Journal of Pharmaceutical Education and Research, 57. https://doi.org/10.5530/ijper.57.2s.24

42. Oliveira, J. R. P., & Lenzi, G. G. (2023). Advances in the use of green and sustainable synthesis to obtain nanomaterials. In IntechOpen eBooks. https://doi.org/10.5772/intechopen.1002866

43. José, B. J. A., & Shinde, M. D. (2024). Colloidal stability and dielectric behavior of eco-friendly synthesized zinc oxide nanostructures from Moringa seeds. Scientific Reports, 14(1). https://doi.org/10.1038/s41598-024-52093-5

44. Gaur, J., et al. (2024). Eco-friendly innovation: Harnessing nature's blueprint for enhanced photocatalysis and antimicrobial potential in multi-structured PN/ZnO nanoparticles. Functional Composites and Structures, 6(1), 15005. https://doi.org/10.1088/2631-6331/ad2c10

45. Lebaka, V. R., Ravi, P., Reddy, M. C., Chandrasekhar, T., & Mandal, T. K. (2025). Zinc oxide nanoparticles in modern science and technology: Multifunctional roles in healthcare, environmental remediation, and industry. Nanomaterials, 15(10), 754. https://doi.org/10.3390/nano15100754

46. Ischenko, A. A., Lazov, M. A., Mironova, E. V., Putin, A. Y., Ionov, A. M., & Storozhenko, P. A. (2023). Analysis of nanoparticles and nanomaterials using X-ray photoelectron spectroscopy. Fine Chemical Technologies, 18(2), 135–167. https://doi.org/10.32362/2410-6593-2023-18-2-135-167

47. Maršík, D., et al. (2024). Synthesis and characterization of lignin-silver nanoparticles. Molecules, 29(10), 2360. https://doi.org/10.3390/molecules29102360

48. Singh, A., BLR, M., & Sagar, M. N. N. (2021). An overview of green synthesis mediated metal nanoparticles preparation and its scale-up opportunities. Journal of Drug Delivery and Therapeutics, 11(6), 304–314. https://doi.org/10.22270/jddt.v11i6.5082

49. Hasan, M. M., Islam, Md. R., Haque, A. R., Kabir, Md. R., Khushe, K. J., & Hasan, S. M. K. (2024). Trends and challenges of fruit by-products utilization: Insights into safety, sensory, and benefits for development of innovative healthy food: A review. Bioresources and Bioprocessing, 11(1). https://doi.org/10.1186/s40643-023-00722-8

50. Toxicity of nanoparticles—Recent advances and new perspectives. (2023). In IntechOpen eBooks. https://doi.org/10.5772/intechopen.111007

51. Nhu, V. T. T., Dat, N. D., Tam, L.-M., & Phương, N. H. (2022). Green synthesis of zinc oxide nanoparticles toward highly efficient photocatalysis and antibacterial application. Beilstein Journal of Nanotechnology, 13, 1108–1119. https://doi.org/10.3762/bjnano.13.94

52. Redjili, S., et al. (2025). Green innovation: Multifunctional zinc oxide nanoparticles synthesized using Quercus robur for photocatalytic performance, environmental, and antimicrobial applications. Catalysts, 15(3), 256. https://doi.org/10.3390/catal15030256

53. Das, P., Ghosh, S., & Nayak, B. (2021). Phyto-fabricated nanoparticles and their anti-biofilm activity: Progress and current status. Frontiers in Nanotechnology, 3. https://doi.org/10.3389/fnano.2021.739286

54. Zanbili, F., & Marjani, A. P. (2025). Innovative green and bio-based approaches for photosensitive nanoparticle synthesis: A review on methodologies, characterization, and applications. Micro and Nano Systems Letters, 13(1). https://doi.org/10.1186/s40486-025-00223-7

55. Nguyen, V. H., Nguyen, H. S., La, D. D., Nguyen, T. T. H., Vu, N. T., & Xuan, C. L. (2024). Use of dialysis membranes for the purification of Fe/Ni and Fe/Cu nanoparticles synthesized from green tea extract. ChemistrySelect, 9(39). https://doi.org/10.1002/slct.202402211

56. Botha, N. L., et al. (2023). Physical properties of computationally informed phyto-engineered 2-D nanoscaled hydronium jarosite. Scientific Reports, 13(1). https://doi.org/10.1038/s41598-022-25723-z

57. Saxena, R., et al. (2025). A review on green synthesis of nanoparticles toward sustainable environment. Sustainable Chemistry for Climate Action, 6, 100071. https://doi.org/10.1016/j.scca.2025.100071

STUDY OF ANTIBACTERIAL AND ANTIFUNGAL EFFICIENCY OF IMPREGNATED CARBON-SILICON MODEL FILTERS

Kudyarova Zh.[1], Baiseitov D.[2*]
[1]"NPTC Zhalyn", Almaty, Kazakhstan
[2]Abai Kazakh National Pedagogical University, Almaty, Kazakhstan
[*]e-mail: baysetov.dauren@gmail.com

Abstract. Air purification is a critical process aimed at removing harmful impurities and ensuring a safe and comfortable environment for human life and activity. This paper presents the antibacterial and antifungal efficacy of impregnated carbon-silicon filters. Antibacterial activity was studied on Bacillus paramycoides and Pseudomonas koreensis strains using the diffusion method on a solid nutrient medium, and antifungal efficacy was studied on strains Fusarium spp. and Penicillium spp. Tests showed that sorbent samples with different active ingredient concentrations exhibited varying levels of bacterial and fungal growth inhibition , with sample No. 2 KRSH+50 I_2 demonstrating the highest activity Optimizing the sorbent composition and increasing the concentration of active components can enhance its antibacterial properties. The developed sorbents have high potential for use in air purification systems with additional protection against bacterial contamination, making them promising for use in areas with increased hygiene and air purity requirements.

Keywords: carbon-silicon filters, antibacterial efficiency, antifungal efficiency, model filters, carbonized rice husk.

Introduction

In the context of rapid urbanization and industrial growth, the issue of maintaining air quality is becoming increasingly important. Air pollution is considered one of the most serious environmental threats of our time, significantly impacting public health, ecosystem health, and climate stability. According to the World Health Organization (WHO), millions of people suffer annually from diseases associated with exposure to air pollution, including acute and chronic respiratory diseases, as well as cardiovascular pathologies. Furthermore, air pollution contributes to an increase in premature mortality and leads to significant economic losses due to increased healthcare costs and decreased productivity [1–4].

Modern technologies for air purification from pathogenic factors include the use of filtration systems, catalytic units, biofilters, and innovative solutions based on nanostructured materials [5–7]. Atmospheric air constantly contains various pollutants, which are divided into mechanical, physical, and biological. Mechanical pollutants include solid particles of various origins—dust, soot, lead, mercury, and combustion products of organic fuels formed during construction, mining, and other industrial activities [8]. Physical pollution is associated with exposure to thermal, noise, electromagnetic, and radioactive radiation. Biological pollutants are caused by the anthropogenic spread of microorganisms in the air. The most toxic components of air pollution are carbon monoxide (CO), nitrogen oxides (NOx), sulfur dioxide (SO2), suspended solids, and various hydrocarbons [9].

The development of process lines in industrial enterprises, the construction industry, and mineral resource extraction sites has led to stricter sanitary and environmental requirements for air quality. This has necessitated updating the regulatory framework and introducing new standards [10]. In Europe, modern standards for assessing the efficiency of air filters have been adopted, including EN 779:1993 and EN 1822:1998 [11,12], which regulate the performance characteristics of filters used in ventilation and air conditioning systems [13].

To impart antibacterial and antifungal properties to filters, they can be impregnated with antimicrobial substances such as iodine or Lugol's solution. These compounds have pronounced antiseptic properties and effectively destroy bacteria, viruses, and fungi on contact. Lugol's solution, a stabilized mixture of iodine and potassium iodide, increases the solubility of iodine and promotes its retention within the filter's porous structure, providing long-lasting antibacterial action. As air passes through the filter, microorganisms meet the iodine-saturated surface, resulting in their destruction [14].

The aim of this work is to investigate the antibacterial and antifungal efficiency of impregnated carbon-silicon model filters.

Materials and methods

To determine the antibacterial activity of the resulting tableted sorbent formulations, two bacterial strains described below were used (Table 1). Given that the Bacillus and Pseudomonas genera are widely distributed in the environment, including water, soil, air, and food products, and are extremely resistant to stress factors, as well as their high adaptability to various conditions, the selected bacterial strains were optimal for testing the sorbent's antibacterial properties. Bacillus paramycoides and Pseudomonas koreensis, isolated from soil, are active strains because they participate in many processes in the rhizosphere, indicating that they are PGPB bacteria with great potential in agriculture. Pure bacterial colonies were subpassaged into sterile liquid nutrient medium to obtain a 24-hour culture and placed in a thermoshaker at 35 ° C and 150 rpm

for 24 hours. After growth, optical density was measured using an APEL PD-303 spectrophotometer. Ten microliters of the liquid medium was then cultured using the Drygalski method on solid MPA nutrient medium in Petri dishes to form a continuous lawn, with tablets then placed in the center. After seeding, the Petri dishes were incubated in a thermostat at 35 ˚C for 24 hours.

Table 1 - Macro- and micromorphological characteristics of identified bacterial strains from museum culture

No.	Name of the strain	Macromorphological characteristics	Micromorphological characteristics
1	*Bacillus paramycoides*	White colony, forms hyphae on solid medium, edges and surface of the colony are uneven	Gram-positive, large rod-shaped morphology 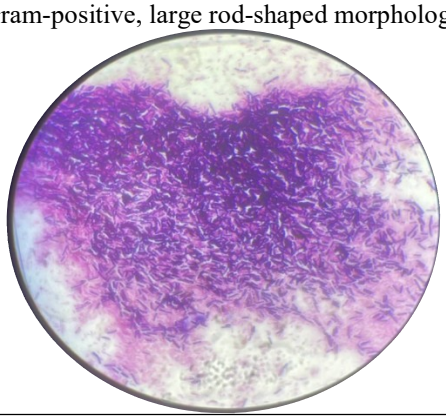
2	*Pseudomonas koreensis*	The colony is pale yellow in color, of medium consistency, with a smooth surface and edge	Gram-negative, rod-shaped morphology 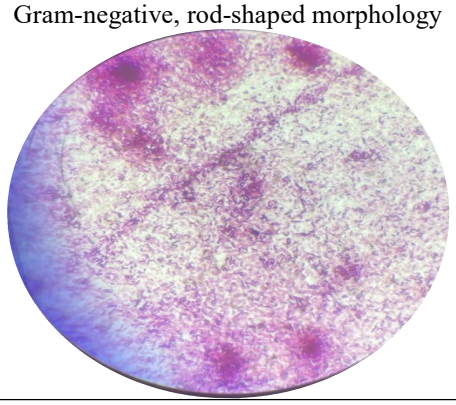

To determine the antifungal activity of the resulting tableted sorbent, two fungal strains described below (Table 2) were used. Given that the Fusarium and Penicillium fungi are widely distributed in the environment, including water, soil, air, and food products, and are extremely resistant to stress factors, as well as their high adaptability to various conditions, the selected fungal strains were optimal for testing the sorbent for antifungal properties. Fusarium spp and Penicillium spp, isolated from soil and spoiled food products, are active and rapidly germinate on organic substrates, indicating their high adaptability to environmental stress factors. Pure fungal colonies were subpassaged into sterile liquid nutrient medium to obtain a 24-hour culture and placed in a thermoshaker at 30 ˚C and 150 rpm for 24 hours. After growth, optical density was measured using an APEL PD-303 spectrophotometer. Then, 100 µl of liquid medium was cultured using the Drygalski method on solid Sabouraud medium in Petri dishes to form a continuous lawn, with tablets placed in the center. After seeing, the Petri dishes were incubated in a thermostat at 30 ˚C for 24 hours.

Table 2 – Drawing of the sorbent on a solid nutrient medium with bacteria

No.	**Name of the strain**	**Macromorphological characteristics**

1	*Fusarium spp*	
2	*Penicillium spp*	

Results and discussions

A carbon-silicon material obtained by carbonizing rice grain husks was chosen for the filter. This choice was determined by the material's porosity, high specific surface area, and pore volume, as well as the presence of finely dispersed carbon and silicon oxide particles. This means the material combines significant sorption capacity for various substances.

The resulting multi-channel block had the following geometric dimensions: 48 mm in diameter and 120 mm in length. It was permeated with 1,000 longitudinal rectangular channels with a cross-section of 1 mm2. Thus, the contact surface of the channels within a single block was 480,000 mm2, or approximately half a square meter (Figure 1).

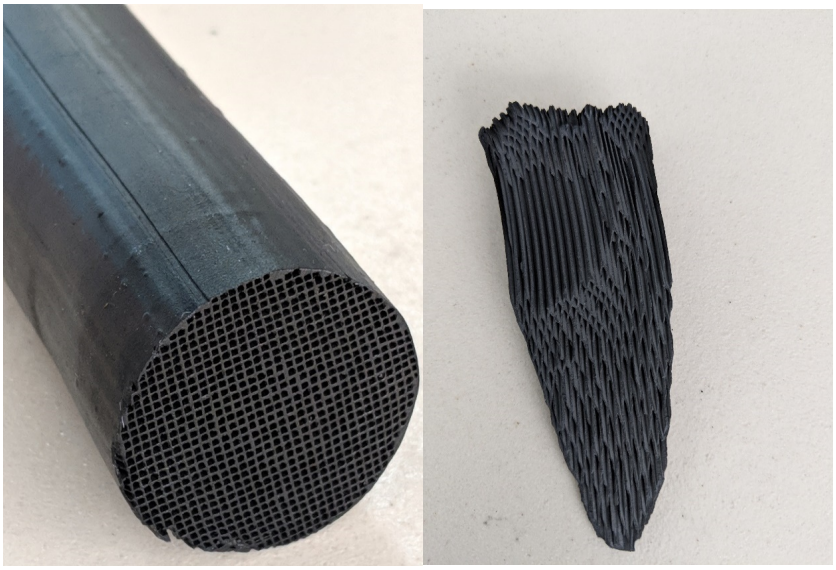

Figure 1 – Model filter made of carbon-silicon sorbent
a) Multichannel block end view b) Block in section

Further research focused on identifying optimal bactericidal additives for impregnating model filters. As demonstrated in previous studies, Nazar solution has proven itself to be a successful bactericide .

Works on The determination of antifungal and antibacterial efficacy was carried out by the Kazakh-German-Chinese International Research Laboratory of Applied Microbiology of the Al-Farabi Kazakh National University.

There is a wide selection of substances with antiseptic properties that can be used as impregnating agents. However, their properties limit their use for air purification.

Iodine and its compounds have been used as antiseptics for over 150 years and are proven remedies. Iodine solution is rightfully considered one of the most common antiseptics in everyday life. However, using iodine preparations for air purification is difficult due to rapid inactivation. This problem can be solved by impregnating the iodine into a nanoporous carbon filter block.

When studying the bactericidal activity of activated carbon samples with varying levels of adsorbed iodine, we discovered that some of them exhibited high antibacterial activity. Iodine compounds possess strong antiseptic properties, effectively killing bacteria, viruses, and fungi upon contact. Lugol's solution, a stabilized mixture of iodine and potassium iodide, increases the solubility of iodine and its retention within the filter's porous structure, ensuring long-lasting antibacterial activity. When air passes through the filter, microorganisms are drawn to the iodine-saturated surface, resulting in their destruction.

Nazar, iodine and Lugol's solutions were chosen as antiseptics. To evaluate the antibacterial effect of a multichannel filter with iodine or Lugol's iodine solution, a comprehensive analysis, including microbiological testing, is necessary. These studies will help determine the filter's effectiveness in killing or retaining pathogenic microorganisms.

Powdered sorbent samples were converted into tablets. For all samples, a 0.5 g sample of powdered sorbent was used and subjected to a pressure of 10 atmospheres for 5 minutes. This resulted in sorbent tablets measuring 0.5 mm (Fig. 2) .

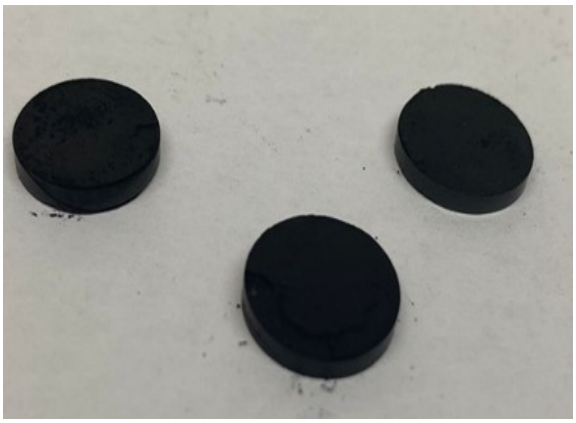

Figure 2 – Sorbent tablets obtained using a press

The test sorbent was prepared from three different variants, consisting of three samples. Table 3 shows the composition of the samples.

Table 3 – Concentration of reagents in the sorbent

No.	Samples
1	KRS + 10% J_2
2	KRS + Lugol
3	KRS + Nazar 5%

Bacillus and Pseudomonas bacteria were selected as bacterial cultures . Bacillus paramycoides and Pseudomonas koreensis, isolated from soil, are active strains as they participate in many processes in the rhizosphere, indicating that they are PGPB bacteria with great potential in agriculture. Table 4 shows the results of the antibacterial activity of carbon-silicon filters.

Table 4 – Antibacterial activity of carbon-silicon sorbents

Sample	Bacillus paramycoides	Pseudomonas koreensis
KRS +10% J_2	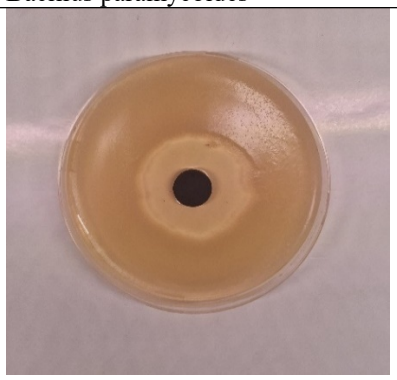 Growth inhibition zone 4 cm	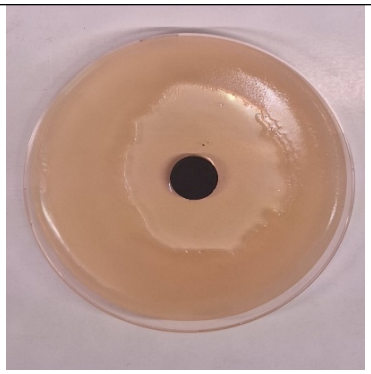 Growth inhibition zone 5 cm
KRS + Lugol	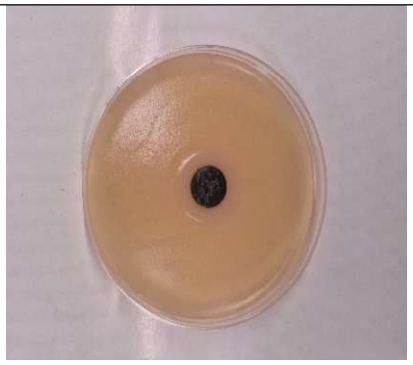 The growth inhibition zone is 1 cm, but the strain has adapted and grown through the initial zone. Bacterial growth on tablets	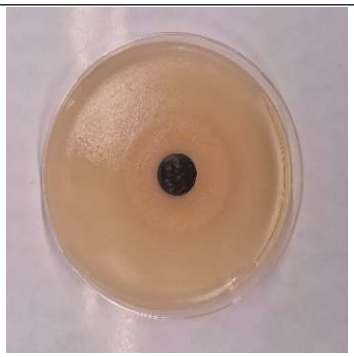 The growth inhibition zone is 2 cm, but the strain has adapted and grown through the initial zone. Bacterial growth on tablets
KRS + Nazar 5%	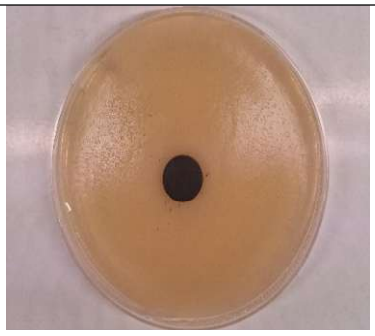 No changes, no antibacterial activity	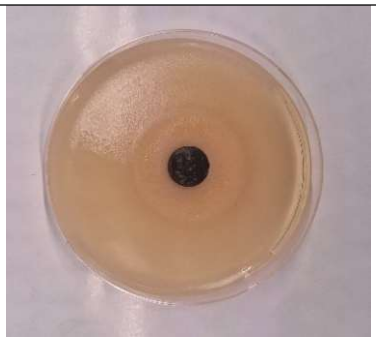 No changes, no antibacterial activity

Thus, sample #3 showed no antibacterial activity on solid nutrient medium containing Bacillus paramycoides and Pseudomonas koreensis strains with a minimum optical density of 0.1 in the initial liquid medium. However, samples #1 and #2 exhibited antibacterial activity against the strains. Sample #2 initially exhibited antibacterial activity, but the tablet concentration was insufficient to inhibit growth. Sample #1 is more suitable for the growth-inhibiting agent and is considered the optimal, recommended composition.

Next, we determined the antifungal efficacy of the sorbents. To determine the antifungal activity of the resulting tablet forms of the sorbent, we used two strains of Fusarium and Penicillium fungi. Fusarium spp. and Penicillium spp., isolated from soil and spoiled food products, are active and rapidly germinate on organic substrates, indicating their high adaptability to environmental stress factors.

The study assessed the antifungal activity of various carbon-silicon sorbent samples against fungal strains of Penicillium spp. and Fusarium spp. The results revealed that sample 3 did not suppress the growth of these microorganisms, indicating a lack of significant antifungal activity. However, samples 1 and 2 demonstrated significant inhibition of fungal growth, with sample 1, containing 10% J2, demonstrating the greatest efficacy, completely suppressing colony development on agar medium. Table 5 shows the results of the antifungal activity of carbon-silicon filters.

Table 5 – Antifungal efficiency of carbon-silicon sorbents

Sample	Penicillium spp	Fusarium spp
KRS +10% J_2	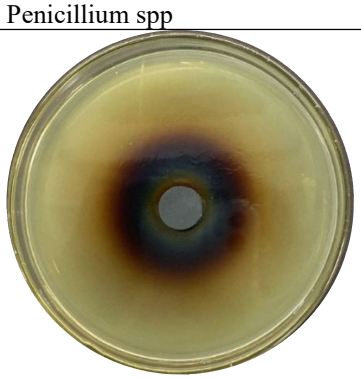 Agar color change due to a component. Inhibition of fungal growth in full volume.	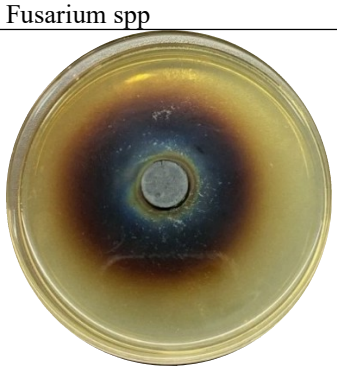 Agar color change due to a component. Inhibition of fungal growth in full volume.
KRS + Lugol	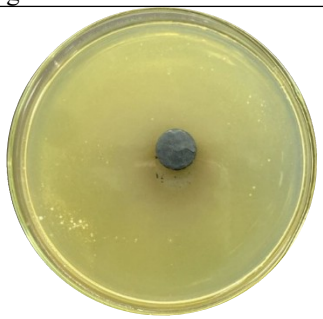 Growth inhibition zone 3 cm	 Growth inhibition zone 1.5 cm
KRS + Nazar 5%	 No changes, no antifungal activity	 No changes, no antifungal activity

Thus, based on the results of the experimental work, the optimal composition of KRSh + 10% J2 was found, demonstrating the highest antibacterial and antifungal efficacy. This result confirms the potential of this sample as a potential fungicidal and antibacterial component for the development of filter materials or other antimicrobial technologies. Additional studies, including the mechanisms of action and long-term stability of the sorbents, will help determine the most effective conditions for their use in air purification systems or materials with antimicrobial properties.

Conclusion

The antibacterial and antifungal efficacy of impregnated carbon-silicon model filters was studied on a test bench. It was found that of the four sorbents tested, sample No. 2 KRSh+50 I_2 exhibited the highest antibacterial and antifungal efficacy, completely suppressing colony growth on an agar mortar.

References

1. Ish, J.L.; Chang, C.J.; Bookwalter, D. B.; Jones, R.R.; O'Brien, K. M.; Kaufman, JD; Sandler, D.P.; White, A. J. Outdoor air pollution exposure and ovarian cancer incidence in a United States-wide prospective cohort study. Environ. Health Perspective. 2024, 132, 107701 . https://pubmed.ncbi.nlm.nih.gov/39352804/

2. Chernobrovkin, IA; Smirnova, LV Air purification from suspended particles: Methods and technologies. Bull. Environ. Saf. 2020, 4, 45–52 .

3. Nowak, DJ; Crane, D. E.; Stevens, J.C. Air pollution removal by urban trees and shrubs in the United States. Urban For. Urban Green. 2006, 4, 115–123 . https://doi.org/10.1016/j.ufug.2006.01.007

4. Li, J.; Zhou, B.; Sun, C. Advances in air purification technologies and challenges for the future. Environ. Sci. Technol. 2018, 52, 12532–12548 .

5. Brook, R.D.; Rajagopalan, S.; Pope, CA; Brook, J.R.; Bhatnagar, A.; Diez-Roux, A. V.; Holguin, F.; Hong, Y.; Luepker, R. V.; Mittleman, MA; et al. Particulate matter air pollution and cardiovascular disease: An update to the scientific statement from the American Heart Association. Circulation 2010, 121, 2331–2378 https://www.ahajournals.org/doi/10.1161/CIR.0b013e3181dbece1

6. Zhang, Q.; He, K.; Huo, H. Cleaning China's air: Prioritizing measures to reduce particulate pollution. Environ. Sci. Technol. 2012, 46, 6521–6522 .

7. Sheoran, K.; Siwal, S. S.; Kapoor, D.; Singh, N.; Saini, AK; Alsanie, W. F.; Thakur, V. K. Air Pollutants Removal Using Biofiltration Technique: A Challenge at the Frontiers of Sustainable Environment. ACS Eng. Au. 2022, 2, 378–396 .

8. Kohse-Höinghaus, K. Combustion in the future: The importance of chemistry. Proc. Combust. Inst. 2020, 38, 1–56 . https://doi.org/10.1016/j.proci.2020.06.375

9. Kianfar, E.; Sayadi, H. Recent advances in properties and applications of nanoporous materials and porous carbons. Carbon Lett. 2022, 32, 1645–1669 . https://doi.org/10.1007/s42823-022-00395-x

10. Roy, A.; Mishra Ch Jain, S.; Solanki, N. A review of general and modern methods of air purification. J. Therm. Eng. 2019, 5, 22–28 . https://doi.org/10.18186/THERMAL.529054

11.EN 779:1993; Particulate Air Filters for General Ventilation—Requirements, Testing, Marking. European Committee for Standardization (CEN): Brussels, Belgium, 1993 .

12.EN 1822:1998; High Efficiency Air Filters (HEPA and ULPA)—Part 1: Classification, Performance Testing, Marking. European Committee for Standardization (CEN): Brussels, Belgium, 1993 .

13.EN 1822:2009; High Efficiency Air Filters-Part 1: Classification, Performance Testing, Marking and Product Documentation. European Committee for Standardization: Brussels, Belgium, 2009 .

14. Chen, M.; Hu, Q.; Wang, X.; Zhang, W. A review on recent trends of the antibacterial nonwovens air filter materials: Classification, fabrication, and application. Sep. Purif. Technol. 2024, 330 Pt B, 125404 . https://doi.org/10.1016/j.seppur.2023.125404

PREPARATION OF HYDROGELS BASED ON ISOPROPYLACRYLAMIDE COPOLYMERS AS DRUG DELIVERY CARRIERS

Rakhmetullayeva R.K.[1*], Toktabayeva A.K.[1]
[1]Al-Farabi Kazakh National University, Almaty, Kazakhstan
[*]e-mail: raikhan.rakhmetullayeva@gmail.com

Abstract. In this work, thermosensitive hydrogels based on N-isopropylacrylamide (NIPAM) and ethylene glycol vinyl ether (EGVE) were synthesized. The hydrogels were prepared by radical copolymerization, and their swelling behavior and temperature sensitivity were investigated. It was found that increasing the EGVE content in the initial monomer mixture led to a higher swelling degree of the hydrogels in water. In addition, increasing the NIPAM content enhanced the thermocollapse behavior of the polymer networks. The interaction of the obtained hydrogels with streptocide was studied, and their potential application as drug delivery carriers and ointment bases was evaluated.

Keywords: thermosensitive hydrogels, N-isopropylacrylamide, ethylene glycol vinyl ether, drug delivery, swelling behavior

Introduction

In recent years, thermosensitive polymer hydrogels have attracted considerable interest in the fields of biomedicine and pharmaceutics. Owing to their ability to respond to changes in environmental temperature, these materials are widely investigated as controlled drug delivery carriers, wound dressing materials, and transdermal therapeutic systems. Hydrogels based on N-isopropylacrylamide (NIPAAm) possess a lower critical solution temperature (LCST), enabling them to change their volume in response to temperature variations and thereby regulate the rate of drug release.

At present, one of the important scientific directions is the regulation of thermosensitive hydrogel properties through the copolymerization of hydrophilic and hydrophobic monomers. It has been established that the structure and swelling properties of NIPAAm-based copolymers depend on the content of hydrophilic fragments in their composition [1]. In addition, the biocompatibility and high-water absorption capacity of hydrogels allow them to be used as materials like soft biological tissues [2]. Recent studies have demonstrated that polymers based on ethylene glycol derivatives can provide prolonged and controlled drug release [3].

In medicine, particularly in the treatment of burns and skin wounds, the demand for biocompatible and effective wound dressing materials is continuously increasing. Thermosensitive hydrogels are considered promising systems for such applications because they maintain a moist environment at the wound site and ensure gradual drug release [4]. Studies conducted over the last decade have investigated the ability of NIPAAm-based hydrogels to form complexes with antibiotics and antiseptic agents, demonstrating their effectiveness in controlled drug delivery systems [5-7]. Furthermore, it has been shown that the swelling behavior and thermocollapse properties of hydrogels in salt solutions depend on their structural characteristics [8].

Therefore, the synthesis of hydrogels based on N-isopropylacrylamide and ethylene glycol vinyl ether, as well as the investigation of their interactions with drugs, are of considerable scientific and practical importance. In the present work, the swelling properties, temperature responsiveness, and streptocide complex formation ability of thermosensitive NIPAAm–EGVE-based hydrogels were investigated.

Materials and methods

Characteristics of starting materials and solvents

N-isopropylacrylamide (NIPAAm) was supplied by “Kohjin” (Japan). The monomer was purified by recrystallization from hexane at 40 °C to remove the inhibitor. The obtained product was kept in air for several days and then dried under vacuum (m.p. = 335–338 K; b.p. = 362 K).

Ethylene glycol vinyl ether (EGVE), with a purity of 99.5%, was dried over freshly calcined potassium carbonate for one week and subsequently distilled three times under vacuum (m.p. = 341.15 K; b.p. = 412 K/96 kPa; nD20 = 1.4360).

Azobisisobutyronitrile (AIBN), analytical grade, was recrystallized twice from absolute ethanol (b.p. = 372 K (experimental data); b.p. = 374 K (reference data)).

N,N′-methylenebisacrylamide (MBAA) (Reanal, Hungary) was used as a crosslinking agent without further purification.

Streptocide (tablet form, Kazakhstan) was used in its as-received pure form without additional purification.

Polymer synthesis

NIPAAm–EGVE copolymers were synthesized via free-radical copolymerization at 333 K in the presence of AIBN. Monomer mixtures with different initial compositions were calculated and prepared as 50–70% aqueous solutions. The prepared solutions were transferred into molybdenum-glass ampoules and purged with argon gas for 10–15 minutes (depending on volume) to remove dissolved oxygen. The ampoules were then placed in an LOIP LT-910 thermostat and kept at the specified temperature until complete gel formation.

After synthesis, the hydrogels were thoroughly washed with distilled water for a long period to remove unreacted monomers and to separate sol and gel fractions.

Physicochemical methods of investigation

To study complex formation with the drug, equilibrium-swollen, tablet-shaped hydrogel samples were immersed in a streptocide solution, and the kinetics of interaction were monitored over time. In addition, the release of streptocide from the hydrogel was investigated by maintaining the samples in solution for approximately one week.

To remove excess streptocide from the obtained complexes, the samples were placed in different buffer solutions, and changes in their volume and optical density were recorded over time.

The relative swelling kinetics of the polymer hydrogels were evaluated using a B-630 cathetometer by monitoring changes in the V/V_0 ratio over time, where V_0 and V correspond to the initial synthesis volume and the equilibrium-swollen volume of the sample, respectively.

FTIR spectra of the EGVE–NIPAAm copolymer and the EGVE–NIPAAm–drug composite were recorded using a "Satellite FTIR Mattson" (USA) spectrometer in the range of 4000–400 cm^{-1}.

The equilibrium swelling degree of the polymer hydrogels was calculated using the following equation:

$$\alpha = \frac{m - m_0}{m_0} \qquad (1)$$

where m is the mass of the equilibrium-swollen polymer sample, and m_0 is the mass of the dry gel.

The mass of the dried sample was determined after vacuum drying in a desiccator until a constant weight was achieved. Mass measurements were carried out using an ISO 9001-certified Sartorius analytical balance (Germany). The swelling degree was determined in several parallel experiments, and the average value was calculated.

The gel fraction yield of the studied hydrogels was calculated using the following equation:

$$G = \frac{m_0}{m_{\text{synth}}} \times 100\% \qquad (2)$$

where G is the gel fraction yield (%), m_0 is the mass of the dried gel (g), and m_synth is the mass of the synthesized gel (g).

The sol fraction was calculated as:

$$S = 100 - G \qquad (3)$$

where S is the sol fraction (%).

The amount of dry polymer content was determined after vacuum drying the samples to constant mass.

Determination of streptomycin concentration

The concentration of streptomycin in solution was determined using a "UV-2401-PC Shimadzu" (Japan) UV spectrophotometer at λ = 235 nm, corresponding to the maximum absorption in the ultraviolet region.

Sorption studies

For the investigation of model substance sorption, crosslinked NIPAAm–EGVE copolymer samples were immersed in streptomycin solution. The amount of sorbed streptomycin was determined from the difference between the initial and final concentrations in solution, using a pre-established calibration curve plotted in D–C coordinates.

To investigate drug release from the hydrogel, streptomycin-loaded hydrogel samples were placed in a cell containing either distilled water or isotonic solution at room temperature. The cell was continuously stirred using a magnetic stirrer. At predetermined time intervals, aliquots of the solution were taken, and the concentration of released streptomycin was monitored by UV spectrophotometry through optical density measurements.

The amount of drug released at time t (W) was calculated using a calibration curve according to equation (4):

$$W = \frac{C}{C_0} \cdot 100\% \qquad (4)$$

where C is the concentration of streptomycin in the surrounding solution at time τ, and C_0 is the initial concentration of streptomycin in the hydrogel.

Membrane diffusion study

For drug release experiments, a dialysis membrane with a molecular weight cut-off of 3500 Da (Medicell International Ltd.) was used. The system was thermostated at 37 °C, and drug release from the hydrogel was monitored using UV spectrophotometry. The concentration of streptomycin in aqueous solutions was determined from a calibration curve (λ = 235 nm) based on optical density as a function of concentration (C, mol/L).

Results and discussion

Currently, a wide range of imported and high-cost pharmaceuticals are widely used in the treatment of various skin diseases and burns. To replace these medicines, the production of biomedical materials—particularly wound dressing materials-based on domestic raw materials and the determination of their optimal formulation remains one of the most relevant challenges.

At the Department of Chemistry and Technology of Organic Substances, Natural Compounds and Polymers at Al-Farabi Kazakh National University, thermosensitive linear and crosslinked copolymers based on ethylene glycol vinyl ether (EGVE) and N-isopropylacrylamide (NIPAAm) have been synthesized via radical copolymerization. The main regularities of their formation and their physicochemical properties have been comprehensively studied [9]. For the preparation of crosslinked copolymers, diethylene glycol divinyl ether was previously used as a crosslinking agent. It was established that the rate of copolymerization of linear polymers is higher, and that NIPAAm units are significantly more reactive compared to EGVE units. The present study represents a continuation of these investigations.

The aim of this work is to obtain hydrogels based on copolymers of N-isopropylacrylamide and ethylene glycol vinyl ether for use as a base for ointment formulations. Unlike the study reported in [9], N,N′-methylenebisacrylamide (MBAA) was used for the first time as a crosslinking agent. Hydrogels were synthesized by varying the molar ratio of monomers in the initial mixture and adjusting the aqueous phase content in the range of 50–70%. An optimal synthesis route was selected based on the experimental results.

The gel fraction yield demonstrates that, as the content of the hydrophilic EGVE monomer in the initial monomer mixture (IMM) increases, both the gel yield and the degree of crosslinking of the hydrogels decrease (Fig. 1a). This indicates that the hydrophobic NIPAAm monomer exhibits higher reactivity compared to the hydrophilic EGVE monomer.

As the proportion of EGVE in the initial monomer mixture increases, the decrease in crosslinking density leads to an increase in the swelling degree of the hydrogels in water, as shown in Fig. 1b. This confirms that water acts as a better solvent for NIPAAm–EGVE polymer hydrogels with higher EGVE content.

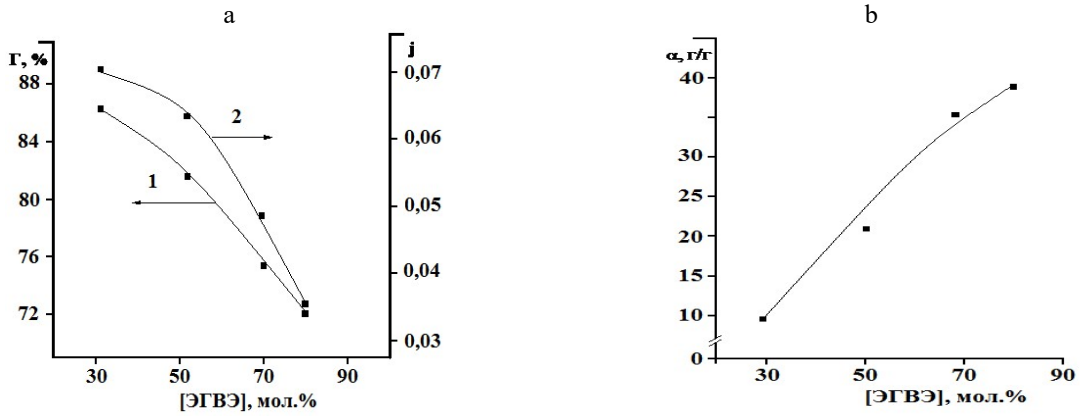

Figure 1 - Dependence of (a) gel fraction and crosslinking degree, and (b) swelling degree in water on the content of EGVE in the initial monomer mixture (IMM)

The curves shown in Figure 2 indicate that the swelling degree is strongly dependent on the copolymer composition. An increase in the content of the hydrophobic NIPAAm component in the initial monomer mixture leads to a decrease in the swelling degree of the resulting hydrogels in water, whereas an increase in the hydrophilic EGVE content results in a corresponding increase in swelling. This behavior can be explained by the reduction in the crosslinking density of the polymer network (Fig. 2).

Compared with the results reported in [9], the hydrogels obtained in this study exhibit noticeably higher swelling capacities. This improvement is attributed to the use of N,N′-methylenebisacrylamide (MBAA) as a crosslinking agent during synthesis, which provides more favorable network formation conditions.

Hydrogels are widely recognized as “smart materials,” as discussed in detail in the literature review. This is primarily due to their high biocompatibility with the human body and their extensive application in controlled drug release systems. Owing to their high-water absorption capacity and soft consistency, they are also used as one of the key components in ointment formulations. Their temperature-dependent drug release behavior is governed by thermosensitive polymer networks. Therefore, investigating the temperature responsiveness of the synthesized copolymers was significant.

To study the thermosensitive behavior of the hydrogels, the effect of temperature on their swelling capacity, specifically on the relative volume change of the copolymers, was investigated. During the thermally induced collapse studies, equilibrium-swollen hydrogel samples in the form of cylinders (3–5 mm in diameter and 2–3 mm in thickness) were placed in a temperature-controlled aqueous cell. The temperature varied from 25 °C to 60 °C in six measurement steps. Changes in the relative volume of the polymer hydrogels were recorded using a V-630 cathetometer (measurement accuracy ±0.1 mm) and evaluated as the V/V_0 ratio.

As shown in Figure 3, an increase in temperature leads to a reduction in the volume of the NIPAAm–EGVE polymer networks, indicating a thermally induced contraction state. This behavior is attributed to the enhancement of hydrophobic interactions involving NIPAAm units, which stabilize a more compact conformation of the copolymer macromolecular chains. Furthermore, increasing the NIPAAm content in the polymer network results in a higher amplitude of thermally induced contraction, and the transition from the swollen to the collapsed state occurs at lower temperatures as the system becomes more hydrophobic.

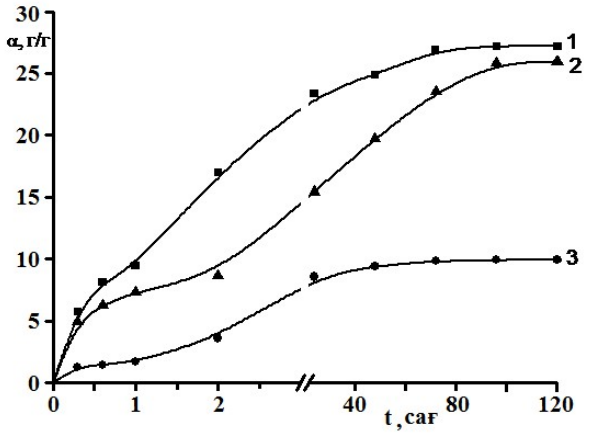

Figure 2 - Swelling kinetics of NIPAAm–EGVE hydrogels in water.

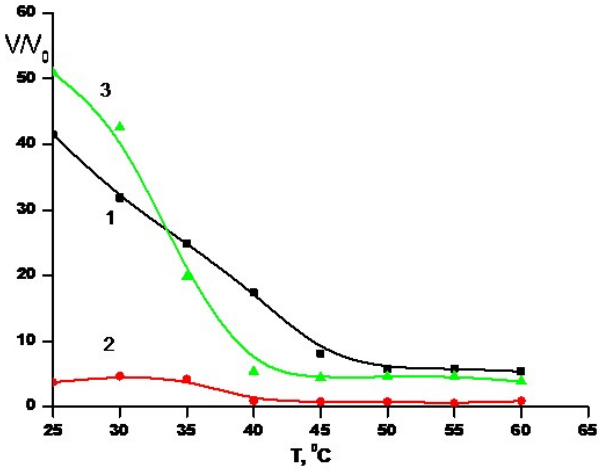

Figure 3 - Effect of temperature on the relative volume of NIPAAm–EGVE copolymer

Burns are injuries to body tissues caused by exposure to high temperatures or certain chemical agents.

The severity of a burn is determined by the depth and area of the injury. First aid in burn cases is primarily aimed at eliminating the effect of the external damaging factor and treating the affected area [10].

Burn injuries are among the most widespread types of trauma worldwide. In the Republic of Kazakhstan alone, approximately 17,000 cases of burn injuries are registered annually. This figure reflects only those patients who seek medical assistance, while an additional 30% receive ongoing treatment. Each year, around 200 people die because of burn-related injuries.

The healing process of burn wounds is generally divided into three stages, depending on the therapeutic approach:

- Phase I – Inflammatory phase. Main characteristics include swelling, significant exudate formation, microbial invasion of the wound area, necrosis development, and disruption of microcirculation.
- Phase II – Regeneration phase (granulation). This stage involves wound cleansing from exudate, reduction of edema, and formation of new connective tissue.
- Phase III – Final maturation phase of connective tissue regeneration. This stage is characterized by the formation of new epithelial tissue on the wound surface.

During the first phase, prevention of secondary infection is critical. In the second phase, the focus is wound cleansing, where the hygroscopic properties (ability to absorb moisture from the environment) of dressing materials play an important role [11].

In this context, polymeric hydrogels have been widely discussed in literature as promising materials for the development of soft contact lenses, controlled and prolonged drug release systems, and transdermal therapeutic systems. Their high-water content in equilibrium state makes their structure highly like human tissues, which provides excellent biocompatibility.

In this study, NIPAAm–EGVE-based hydrogels were investigated as potential drug carriers and as a base material for ointment formulations, with particular emphasis on their interaction with drug substances. Streptocide was selected as the model drug. Streptocide is a broad-spectrum antibacterial agent. Its mechanism of antimicrobial action is associated with antagonism toward para-aminobenzoic acid (PABA), a structurally similar compound. Streptocide is taken up by microbial cells, where it competes with PABA and inhibits its incorporation into dihydrofolic acid. It also competitively inhibits the enzyme dihydropteroate synthase, which is responsible for the incorporation of PABA into dihydrofolic acid. As a result, the synthesis of dihydrofolic acid is disrupted, leading to a decrease in the formation of tetrahydrofolic acid, which is essential for the synthesis of purines and pyrimidines. This ultimately inhibits microbial growth and reproduction, producing a bacteriostatic effect [45].

In this work, the swelling kinetics of the NIPAAm–EGVE crosslinked network in streptocide solutions with different NaCl concentrations, as well as in alcohol, was investigated (Fig. 4). It was found that, regardless of the composition of the NIPAAm-based copolymer, the hydrogels did not swell in alcohol, which is attributed to the precipitation effect of alcohol on the linear structure of the hydrogel network [9].

It was also observed that increasing the concentration of NaCl leads to different swelling behaviors of the hydrogel. As the concentration of low-molecular solutes increases, the swelling degree of the hydrogel decreases, which is explained by the thermodynamically unfavorable interactions between the hydrophobic groups in the copolymer and the surrounding medium.

This is further confirmed by the fact that increasing the proportion of NIPAAm units in the copolymer results in a greater decrease in swelling in saline solutions. However, in systems with a high content of NIPAAm units and at high salt concentrations, the hydrogel exhibits an initial swelling within the first 1.5–2 hours, passing through a maximum. This initial swelling is attributed to the adsorption of low-molecular species on the hydrogel surface, leading to surface contraction of the polymer network. As a result, NaCl ions can penetrate the internal pores of the hydrogel network, causing a temporary increase in swelling during the initial stage.

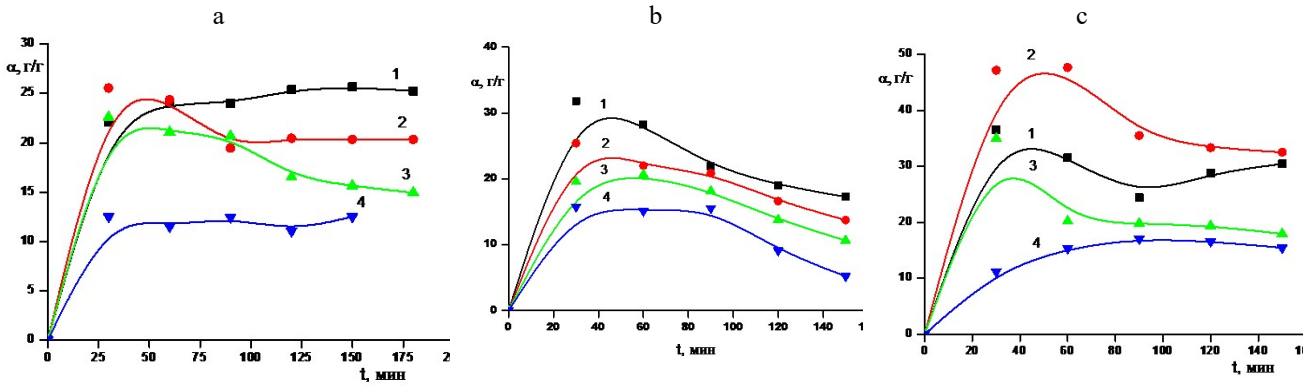

Figure 4 - Swelling kinetics of NIPAAm–EGVE hydrogels in different media.
Initial monomer feed ratio (IMM): [NIPAAm]:[EGVE] = 30:70 (a); 50:50 (b); 70:30 (c), mol.%.
NaCl concentrations: 0.45 (1); 0.9 (2); 1.8 (3); and alcohol (4).

To obtain hydrogel-based ointment matrices from isopropylacrylamide copolymers, the interaction patterns between the drug substance and the polymer network were investigated.

For studying complex formation with the drug (DS), equilibrium-swollen tablet-shaped hydrogel samples were immersed in a streptocide solution, and the kinetics of the interaction were monitored over time (Fig. 5). The experiments were carried out using UV spectrophotometry.

The obtained results showed that complex formation between the drug and the copolymer increases with both (i) the percentage of NIPAAm units in the hydrogel composition and (ii) the ionic strength of the medium. This behavior is explained by the fact that, in addition to coordination interactions between streptocide and the polymer matrix, hydrophobic interactions also contribute significantly to complex formation.

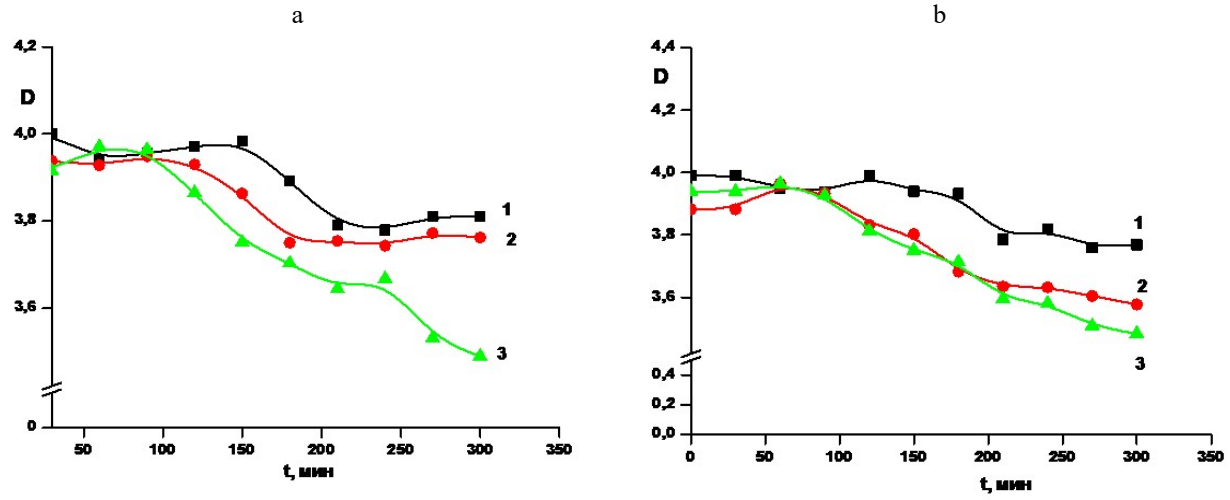

Figure 5 - Sorption kinetics of drug substance by NIPAAm–EGVE hydrogels.
Initial monomer feed ratio (IMM): [NIPAAm]:[EGVE] = 30:70 (1); 50:50 (2); 70:30 (3), mol.%.
Drug concentration: 0.1% (a); 0.05% (b).

Conclusion

In this work, water-swellable copolymers based on N-isopropylacrylamide (NIPAAm) and ethylene glycol vinyl ether (EGVE) were successfully synthesized. The influence of temperature on the hydrogel systems was investigated. It was found that increasing the proportion of NIPAAm units in the copolymer composition accelerates the thermally induced collapse (thermocollapse) behavior of the hydrogels.

To evaluate the potential application of the obtained hydrogels as ointment bases, their interaction with a model drug substance was studied. Streptocide was used as the model drug. It was established that an increase in the NIPAAm content in the hydrogel composition leads to enhanced ability of the polymer network to form complexes with the drug substance.

References

1. Hoare, T. R., & Kohane, D. S. (2008). Hydrogels in drug delivery: Progress and challenges. Polymer, 49(8), 1993–2007. https://doi.org/10.1016/j.polymer.2008.01.027

2. Li, J., & Mooney, D. J. (2016). Designing hydrogels for controlled drug delivery. Nature Reviews Materials, 1, 16071. https://doi.org/10.1038/natrevmats.2016.71

3. Zhang, Y. S., & Khademhosseini, A. (2017). Advances in engineering hydrogels. Science, 356(6337), eaaf3627. https://doi.org/10.1126/science.aaf3627

4. Ahmed, E. M. (2015). Hydrogel: Preparation, characterization, and applications. Journal of Advanced Research, 6(2), 105–121. https://doi.org/10.1016/j.jare.2013.07.006

5. Kamaly, N., Yameen, B., Wu, J., & Farokhzad, O. C. (2016). Degradable controlled-release polymers and polymeric nanoparticles: Mechanisms of controlling drug release. Chemical Reviews, 116(4), 2602–2663. https://doi.org/10.1021/acs.chemrev.5b00346

6. Qiu, Y., & Park, K. (2012). Environment-sensitive hydrogels for drug delivery. Advanced Drug Delivery Reviews, 64(Suppl.), 49–60. https://doi.org/10.1016/j.addr.2012.09.024

7. Pinelli, F., Perale, G., & Rossi, F. (2020). Coating and functionalization strategies for nanogels and nanoparticles for selective drug delivery. Gels, 6(1), 6. https://doi.org/10.3390/gels6010006

8. Li, X., Sun, Q., Li, Q., Kawazoe, N., & Chen, G. (2018). Functional hydrogels with tunable structures and properties for tissue engineering applications. Frontiers in Chemistry, 6, 499. https://doi.org/10.3389/fchem.2018.00499

9. Ulantay Nakan, Mun, G. A., Yeligbayeva, G. Z., & Bieerkehazhi, S. (2020). Hydrogels based on N-isopropylacrylamide and 2-hydroxyethylacrylate: Synthesis, characterization, and investigation of their antibacterial activity. Polymer International, 69, 1220–1226. https://doi.org/10.1002/pi.6065

10. Klouda, L., & Mikos, A. G. (2008). Thermoresponsive hydrogels in biomedical applications. European Journal of Pharmaceutics and Biopharmaceutics, 68(1), 34–45. https://doi.org/10.1016/j.ejpb.2007.02.025